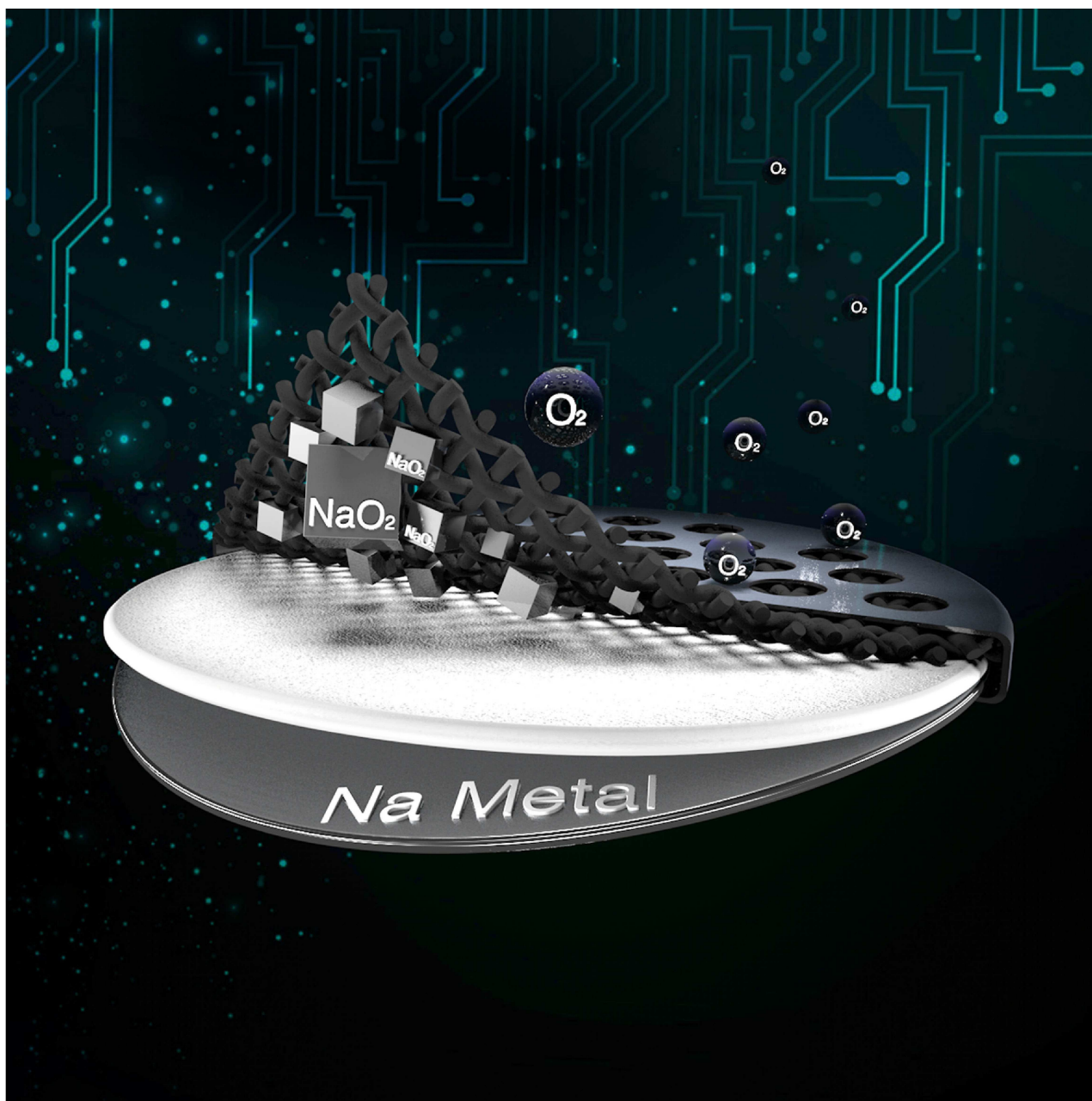




Recent Development of Aprotic Na-O₂ Batteries

Shuo Zhao⁺^[a] Bin Qin⁺^[b] Kwong-Yu Chan,^{*[b]} Chi-Ying Vanessa Li,^[b] and Fujun Li^{*[a]}



Rechargeable aprotic sodium-oxygen (Na-O₂) batteries that can operate with low overpotential (< 200 mV) have attracted extensive attention. A lot of progress in performance and understanding of Na-O₂ batteries has been made, but there remain significant challenges. Herein, a critical review is given to suggest directions of further improvement.

The development of batteries with high energy density and low costs involves chemistry beyond lithium-ion batteries. Rechargeable sodium-oxygen ($\text{Na}-\text{O}_2$) batteries make two essential steps forward: i) replacing Li by Na to remove the bottleneck in resources supply and ii) using oxygen from air to raise the theoretical energy density. A lot of progress has been made in performance and understanding of $\text{Na}-\text{O}_2$ battery since its first report in 2012. However, there remain significant challenges,

such as the instability of discharge products, dendrite growth of Na metal, and the crossover of superoxide. A timely review is given here to summarize the challenges encountered in the components of the $\text{Na}-\text{O}_2$ battery. Insights are offered on sodium anode protection, morphology dynamics at the cathode, amphibian presence of superoxide, and the roles of electrolyte. Bright prospects in further development of aprotic $\text{Na}-\text{O}_2$ batteries are envisioned.

1. Introduction

1.1. Two Steps Beyond Li-Ion Batteries

Materials for viable systems beyond lithium-ion batteries (Li-ion) are currently under intensive study to satisfy the high-growth markets in electric vehicle and energy storage systems. Although Li-ion batteries are widely used in mobile devices, there are fundamental barriers limiting further penetration in markets of energy storage devices. Sodium-air ($\text{Na}-\text{O}_2$) battery system is one of the many potential solutions. The $\text{Na}-\text{O}_2$ battery system makes two important steps beyond the Li-ion battery technology: i) replacing lithium with the naturally abundant sodium removes the bottleneck in resources supply chain; ii) replacing solid redox active material in cathode by oxygen from air eliminates the weight gaining effect of heavy transition metal atoms.^[1] There is, however, still the need to use an electrode, e.g. carbon electrode which has definite mass. The electrode also needs reasonable porosity and therefore lowers the energy density on a volumetric basis. A typical aprotic $\text{Na}-\text{O}_2$ battery is composed of sodium metal anode, electrolyte, separator, carbon cathode, and an O_2 source as shown in Figure 1. During discharge, Na at anode is converted to Na^+ in the electrolyte, while O_2 is reduced at the cathode in presence of Na^+ forming NaO_2 or Na_2O_2 or other products with the overall battery reactions.

According to Equation 1 and 2 of Figure 1, the $\text{Na}-\text{O}_2$ system operates at ~ 2.3 V. Though this value is lower than that of the Li-ion and $\text{Li}-\text{O}_2$ batteries as shown in Table 1, the present $\text{Na}-\text{O}_2$ battery has much lower overpotential achieved for discharge/charge than the $\text{Li}-\text{O}_2$ system, 0.2 vs 1.0 V, thus offering a higher round-trip efficiency. As sodium is the 6th

most abundant element of Na on earth, deployment of $\text{Na}-\text{O}_2$ battery at large scale is favored with low materials costs expected.

While the $\text{Na}-\text{O}_2$ battery is theoretically attractive, the changes at anode and cathode have faced serious technical challenges. Though the $\text{Na}-\text{O}_2$ battery has an oxygen cathode analogous to the $\text{Li}-\text{O}_2$ battery with similar electrochemical reactions expected, recent research suggests otherwise. Sodium superoxide is the stable product observed as opposed to lithium peroxide in the $\text{Li}-\text{O}_2$ battery. As monitored by in situ differential mass spectroscopy (DEMS), $\text{Li}-\text{O}_2$ and $\text{Na}-\text{O}_2$ batteries with identical electrolyte have different oxidation and electrochemical products.^[2] The 2-electron electrochemical reaction per O_2 molecule in the $\text{Li}-\text{O}_2$ battery indicates formation of Li_2O_2 , while a one electron per O_2 molecule in the $\text{Na}-\text{O}_2$ battery corresponds to formation of NaO_2 . In addition, trace amounts of sodium acetate (NaOAc) and NaOH are detected, while NaF and Na_2CO_3 are not detected.^[2] Lithium oxide (Li_2O) is observed as a minor product in $\text{Li}-\text{O}_2$ batteries but the parallel of Na_2O is not observed in $\text{Na}-\text{O}_2$ batteries.

Still in its infancy stage, the $\text{Na}-\text{O}_2$ battery deserves a timely review of its technological status and issues arise from the principles of its operation. In this review, we discuss the reaction mechanism and the related issues of materials stability for the $\text{Na}-\text{O}_2$ battery components: Na metal, Na-air cathode, and electrolyte. Where possible, we refer to the better-known $\text{Li}-\text{O}_2$ battery or the equally challenging $\text{Li}-\text{O}_2$ battery for comparison.

2. Challenges at the Anodes

2.1. Sodium Anodes

The anode is the sodium source of a $\text{Na}-\text{O}_2$ battery, where the Na/Na^+ redox reaction takes place. In pursuing the maximum specific energy and power density, sodium metal is used as the anode in $\text{Na}-\text{O}_2$ batteries. However, owing to the high reactivity and dendrite formation, sodium metal may not be an ideal anode. The active dendrite of sodium can result not only in limited battery performance, but also potential hazard.^[3] Dendrites originate from inhomogeneous sodium deposition in charging processes. Uncontrollable dendrites can pierce through the separator reach the cathode, thus causing short circuit, which strongly limits the cycling performance or even starts a blaze.^[4] Moreover, due to the high reductivity and

[a] S. Zhao,[†] Prof. F. Li
Key Laboratory of Advanced Energy Materials Chemistry (Ministry of Education)
Renewable Energy Conversion and Storage Center (RECAST)
College of Chemistry
Nankai University
Tianjin, 300071, P.R. China
E-mail: fujunli@nankai.edu.cn

[b] B. Qin,[†] Prof. K.-Y. Chan, Dr. C.-Y. V. Li
Department of Chemistry
University of Hong Kong
Pokfulam Road, Hong Kong, P.R. China
E-mail: hrsccky@hku.hk

[†] These authors contributed equally to this work.

An invited contribution to a Special Collection dedicated to Metal-Air Batteries



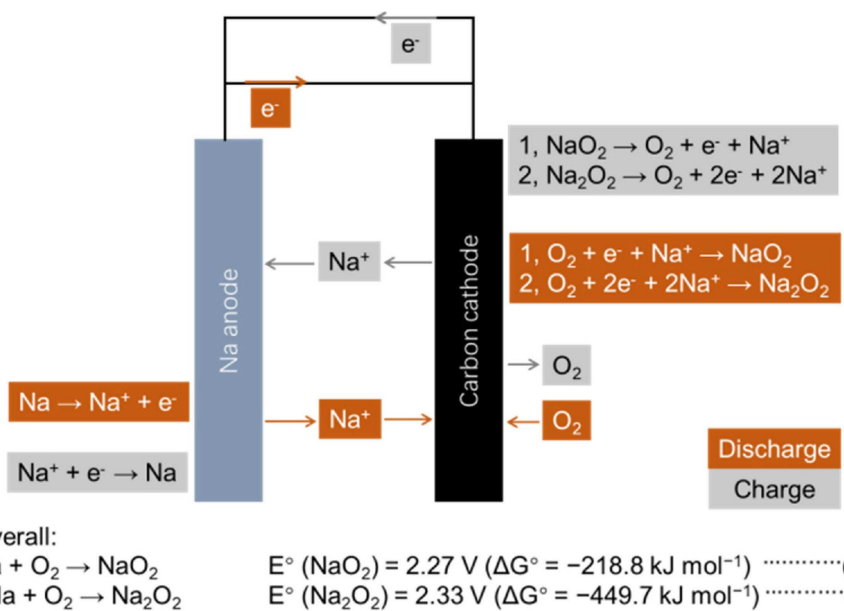


Figure 1. Operation principles of an aprotic $\text{Na}-\text{O}_2$ battery.

reactivity of sodium, it can easily react with solvents^[5] and solutes including salts,^[6] additives,^[7] oxygen, and superoxide radicals.^[8] Apart from consumption of electrolytes, side reactions also decline the cycling efficiency of sodium. As a result, excessive sodium is required for long cycles with penalty of energy density.

2.1.1. Dendrite Formation and Suppression

Dendrite is one of the most serious problems of metallic anodes in alkali-metal battery systems, such as $\text{Li}-\text{O}_2$,^[9] $\text{Li}-\text{S}$,^[10] $\text{Na}-\text{O}_2$,^[3] $\text{K}-\text{O}_2$ batteries^[11] etc. Dendrite formation limits the cycling performance of a $\text{Na}-\text{O}_2$ battery, which is commonly



Shuo Zhao obtained his B.S. degree from Tianjin University and Nankai University in 2018. He is pursuing his M.S. at Key Laboratory of Advanced Energy Materials Chemistry (KLAEMC, Ministry of Education), Nankai University. His research interests focus on sodium anode and $\text{Na}-\text{O}_2$ batteries.



Bin Qin obtained his B.S. degree from Lanzhou University in 2014 and M.E. degree from Nankai University in 2017. He is pursuing his Ph.D. at the Department of Chemistry, The University of Hong Kong. His research interests focus on aprotic $\text{Na}-\text{O}_2$ batteries.



Kwong-Yu Chan is a professor in the Department of Chemistry, The University of Hong Kong. He obtained his B.Sc. from University of Alberta in 1979, Ph.D. degree from Cornell University in 1988. His research interests include nanomaterials, membrane, fuel cells, batteries, and catalysts.



Chi-Ying Vanessa Li is a Research Assistant Professor at the University of Hong Kong. She obtained a Ph.D. degree from University of New South Wales in 2009, followed by a postdoctoral position at The University of Hong Kong. Her research interests include nanomaterials for catalysis, and advanced battery systems.



Fujun Li is a Professor at Key Laboratory of Advanced Energy Materials Chemistry (KLAEMC, Ministry of Education), Nankai University. He obtained his Ph.D. degree from The University of Hong Kong in 2011, and then worked as a postdoc fellow at the University of Tokyo and National Institute of Advanced Industrial Science and Technology (AIST, Tsukuba), Japan till 2015. His research interests include energy materials chemistry, $\text{Li}-\text{O}_2$ (air) batteries, and Li-ion batteries.

Table 1. Comparison of the basic characteristics of Na–O₂ batteries against the Li-ion batteries and the Li–O₂ batteries.

| | Na–O ₂ batteries | Li-ion batteries | Li–O ₂ batteries |
|----------------------------|---|---|--|
| Active Redox Materials | Na, O ₂ | Li, LiCoO ₂ | Li, O ₂ |
| Abundance of the component | Na is 6th abundant on earth's crust (2.3%) | Co is 32nd abundant on earth's crust (0.003 %) | Li is 33rd abundant on earth's crust (0.0017 %) |
| Active Redox Reaction | Na + O ₂ → NaO ₂ | Li _{0.5} CoO ₂ + 0.5Li → LiCoO ₂ | 2Li + O ₂ → Li ₂ O ₂ |
| Theoretical Capacity | 488 mAh/g | 137 mAh/g | 1168 mAh/g |
| Standard potential | 2.27 V | ~4.0 V | 2.96 V |
| Theo. Energy Density | 1108 Wh/kg(NaO ₂) | 548 Wh/kg(LiCoO ₂) | 3458 Wh/kg(Li ₂ O ₂) |
| Overpotential | < 200 mV | | > 1000 mV |
| Serious Challenges | NaO ₂ stability, Na stability, Na dendrite | Li dendrite, Li stability, low capacity | Li ₂ O ₂ stability, Li dendrite, large overpotential |

attributed to inhomogeneous deposition of sodium ions in the charging process. i) Ununiform charge distribution from the uneven surface of a sodium anode, ii) heterogeneous composition and ununiform morphology of solid-electrolyte interface (SEI), and iii) excessive local current density are considered as the origins of dendrites. Needlelike, branched, mossy, and cubic sodium dendrites have been obtained at different current densities and in different electrolytes,^[4a,12] which lead to short circuit and dead sodium, resulting in limited cyclability and low Coulombic efficiency. Up to now, plenty of strategies have been proposed to suppress dendrite formation and growing, including i) special current collectors that induce uniform sodium deposition, ii) modified SEI by electrolyte additives or pretreatment, iii) functional separators with high mechanical modulus to prevent dendrite piercing, as depicted in Figure 2.

Specially designed current collectors are made to mitigate the large volume change and guide the uniform Na⁺

deposition. By utilizing porous electrode matrix, the spots for Na nucleation are increased, hence decreasing the local current density and the flux distribution of Na⁺. Currently, carbon fibers,^[17] reduced graphene oxide (rGO),^[18] porous Al^[19] and Cu^[13] etc. have been reported as the current collecting matrix. In 2017, Lu *et al.*^[13] demonstrated that the electrochemical deposition stability can be significantly promoted by a 3D Cu current collector with thin nanowires (< 40 nm) in Figure 2a. The Na deposited anode provides sufficient charge centers to distribute Na ion flux, demonstrating enhanced Na plating/stripping stability. Porous Al current collector deposited with Na was reported by Liu *et al.*^[19] which enables the Na–O₂ battery with 1 M NaPF₆ in diglyme electrolyte to maintain capacity of 600 mAh cm⁻² over 200 cycles.

In situ formed SEI is reported to be an effective way to suppress the sodium dendrite. On an uneven surface of sodium metal, electric field and ion concentration gradients are larger

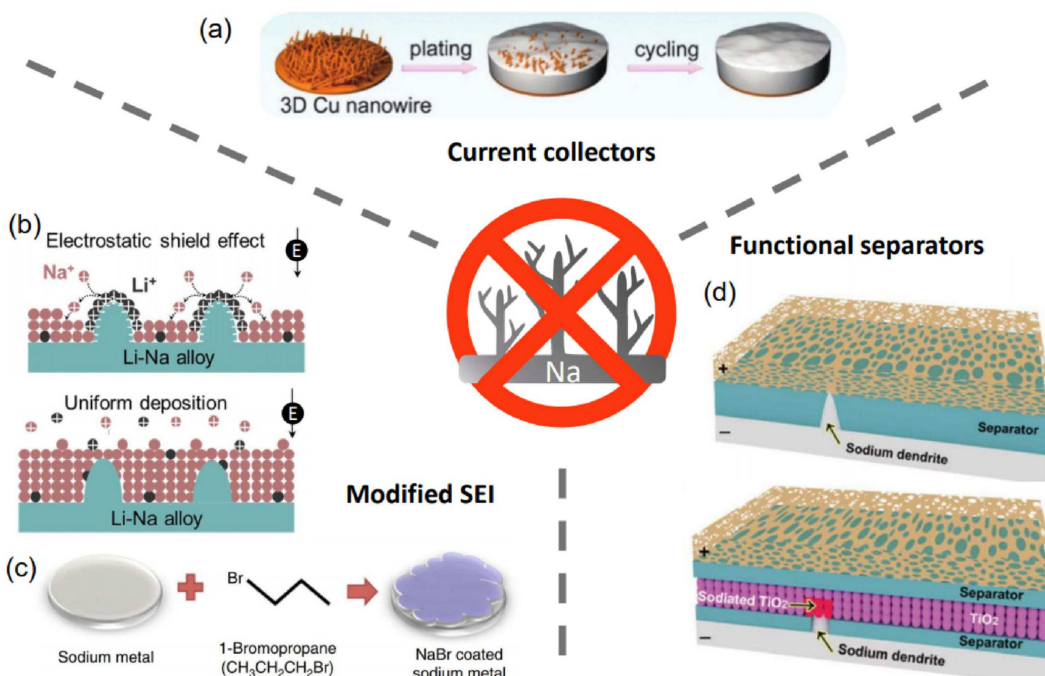


Figure 2. Illustration of dendrite suppression strategies, including (a) 3D Cu nanowire current collectors,^[13] (b) modified SEI with electrostatic shielding effect of Li⁺,^[14] (c) NaBr-containing artificial SEI^[15] and (d) functional separators with TiO₂ nanoparticle sandwiched.^[16] Reproduced with permission from ref. 13–16. Copyright 2017, 2018 Royal Society of Chemistry and Nature Publishing Group.

at tips, where Na^+ prefers to nucleate. To alleviate the tip effect, a self-healing electrostatic shield mechanism was proposed.^[20] As displayed in Figure 2b, a cationic additive of Li^+ with low reduction potential is introduced to the electrolyte, which is thermodynamically unfavorable to get reduced comparing with Na^+ . The Li^+ forms a positively charged electrostatic shield at the nucleation tips. The shield forces Na^+ to get reduced and deposit at the substrate, preventing dendrite growth. The sodium anode protected by electrostatic shield of Li^{+} ^[14] and K^{+} ^[21] demonstrates boosted cycling stability. On the other hand, robust protective SEI was reported through in-situ generation. Seh *et al.*^[22] reported the superior reversibility of Na striping and plating in NaPF_6 in glymes. The compact SEI containing NaF and Na_2O is generated from the decomposition of glyme solvents and NaPF_6 at the surface of Na. The SEI possesses high ionic conductivity and protects sodium from further corrosion, resulting in ultrahigh Coulombic efficiency and low voltage hysteresis in $\text{Na} \parallel \text{Na}$ symmetric batteries. Artificial pretreatment is also applied for a protective SEI. In 2017, Choudhury and co-workers^[15] introduced SEI of NaBr, from a reaction of the sodium anode with bromopropane to undergo Wurtz reaction in Figure 2c. The NaBr interface with fast ion transportation suppresses dendrite formation and side reactions. In order to guide uniform ion flux distribution, a polyvinylidene difluoride fiber film (f-PVDF) is introduced to the surface of sodium anode.^[23] With strong polar C–F function groups, f-PVDF provides strong affinity to electrolyte solutions, of which high ionic conductivity and good wettability endow the $\text{Na}–\text{O}_2$ battery with high rate capability and enhanced cyclability.

To physically prevent the dendrite penetration, a shear modulus of separators is about twice of the metal dendrites.^[24] The conventional separators, like glass fiber and celgard separators, with low mechanical modulus are unable to inhibit dendrite piercing, shown in Figure 2d. Increasing the thickness of glass fiber or celgard separators can improve the cycle life of $\text{Na}–\text{O}_2$ batteries, but penetration still occurs after deep discharging and charging.^[4a] In 2015, Bi and co-workers^[4b] introduced a Nafion- Na^+ membrane to a glass fiber separator in $\text{Na}–\text{O}_2$ batteries. The good mechanical strength of Nafion membranes efficiently suppress the dendrite penetration, and the cycle life is significantly improved to 120 cycles. Besides, a polypropylene-TiO₂-polypropylene (PP–TiO₂–PP) sandwiched separator in Figure 2d,^[16] and mechanically reinforced glass microfiber frameworks with either aluminum oxide (to form α -RGMF) or sodium beta-alumina (to form β -RGMF) particles^[25] are reported with a prolonged cycle life in $\text{Na}–\text{O}_2$ batteries.

2.1.2. Side Reactions

Owing to the high reactivity, sodium anode suffers from various side reactions with the components in electrolytes, such as solvent molecules, salt anions, possible additives, impurity like H_2O , dissolved O_2 and crossover O_2^- in Figure 3. These side reactions consume both the sodium anode and electrolyte, leading to low reversibility, increasing internal resistance and

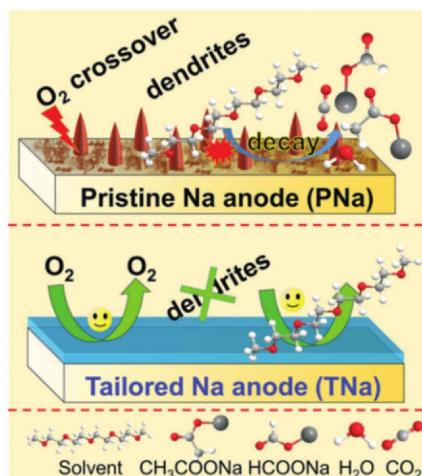


Figure 3. Illustration of problems (O_2 crossover, dendrite formation, and electrolyte decay) on pristine Na anode in $\text{Na}–\text{O}_2$ battery and tailored Na anode against side reactions between the electrolyte and Na anode.^[27] Reprinted with permission from ref. 27. Copyright 2017 Wiley-VCH Verlag GmbH & Co. KGaA.

inducing termination of batteries. Bi *et al.*^[4b] applied a small amount of sodium for cycle efficiency test in an electrolyte of sodium triflate (NaOTf) in dimethoxy ethane (DME). The reversibility efficiency of Na is 60–80%, indicating plenty of sodium is consumed by side reactions. Furthermore, after 120 cycles,^[4b] the sodium anode is fully consumed by corrosion from the electrolyte and O_2 . At anode, NaO_2 and Na_2O_2 were generated by the crossover O_2 , while NaOH and Na_2CO_3 originated from decomposition of salts and electrolyte. Besides, H_2O as a common impurity in the electrolyte can generate an SEI with NaOH as the dominant component, resulting in an increased impedance.^[26]

To protect the sodium anode from the crossover O_2 , artificial protective layers and modified SEI are proven to be effective. Li *et al.*^[8] introduced a carbon paper (CP) at the surface of sodium anode, which acted as a sacrificial protective interlayer. Carbon paper gains a pseudo-equal potential at Na metal surface, and the crossover O_2 and O_2^- prefers to react with CP instead of Na anode. Wu *et al.*^[27] reported $\text{Na}–\text{O}_2$ batteries with superior stability using a tailored sodium anode, which was prepared by cycling with additive of fluoroethylene carbonate (FEC) in a symmetric battery. In the pretreatment process, FEC was preferentially reduced to form the passivation film on Na anode, suppressing the electrolyte decomposition and the crossover O_2 in the $\text{Na}–\text{O}_2$ batteries in Figure 3. The generated SEI film was characterized by XPS, indicating that NaF is the main component.

2.2. Other Anode Materials

Alternative anode materials favor to realize stable $\text{Na}–\text{O}_2$ batteries. Plenty of efficient anode materials are reported,^[29] including carbon-based anode,^[30] Bi,^[31] Co doped FeS₂,^[32] SnP *et al.*^[33] However, their applications in $\text{Na}–\text{O}_2$ batteries are

limited. Bender *et al.*^[28] replaced the sodium anode with a sodiated carbon electrode, as shown in Figure 4a,b. The carbon gas diffusion layer, which was usually used as cathode material, was sodiated in a coin battery against a sodium counter electrode and then used in a full battery with a conventional carbon cathode; it shows a sloping trend of discharging/charging potentials. In a deep cycling experiment, Na–O₂ batteries with the sodiated carbon anode demonstrated better capacity retention and improved cycling stability. Dilimon *et al.*^[34] reported dimethyl sulfoxide (DMSO)-based Na–O₂ batteries using pre-sodiated antimony (Sb:Na) anode to prevent the reaction between DMSO and sodium metal. Owing to the electrochemical potential of the Na–Sb alloy (0.7–0.8 V vs Na/Na⁺), the discharge potential decreases to ~1 V. Recently, a novel bimetallic Li–Na oxygen battery was introduced by Ma *et al.*^[14] Different from the Na–Sb alloy, the Li–Na alloy is a eutectic alloy with the two components retaining their individual crystal structures. Despite the immiscibility of the Li–Na alloy, it exhibited the similar reactivity and electrolyte compatibility of Li⁺ and Na⁺ at no cost of specific capacity. As illustrated in Figure 4c, the Li–Na alloy demonstrated enhanced chemical stability in O₂ atmosphere and electrolytes. The strong corrosion resistance originates from the alloy's inherent charac-

teristics. Providing the volume expansion caused SEI crack, 1,3-dioxolane (DOL) was added to the electrolyte to form a robust and highly elastic SEI layer.

3. Challenges at the Cathodes

3.1. Discharge Products

Since room-temperature aprotic Na–O₂ batteries were first reported in 2012, discharge products including NaO₂,^[25,35] Na₂O₂,^[36] Na₂O₂·2H₂O,^[37] Na₂CO₃,^[38] and NaOH^[38a,39] have been identified under more or less similar experimental conditions. They are technologically and scientifically important to understand how these different products are formed, which will not only favor designing better Na–O₂ batteries but also provide profound understanding of aprotic metal-air batteries.

As shown in Figure 5, NaO₂ has been proved to be a main discharge product in ether-based electrolytes by many different research groups, and the existence of NaO₂ is clearly characterized by X-ray diffraction spectroscopy (XRD), Raman spectroscopy (Raman), scanning electron microscope (SEM), gas pressure monitoring and singular charge profiles. It is reason-

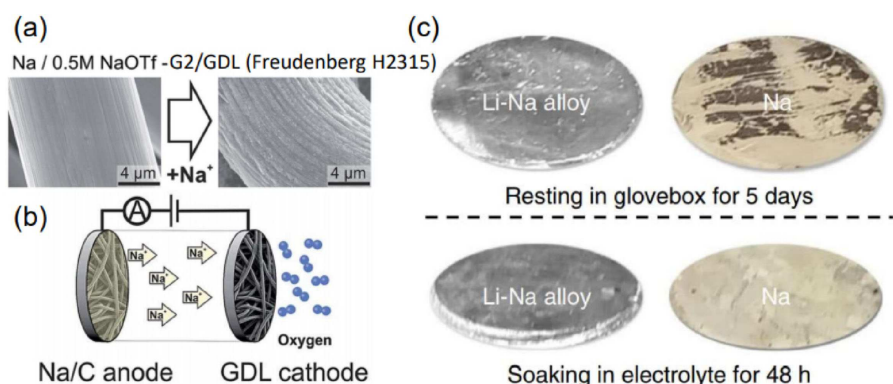


Figure 4. Other sodium anode materials. (a) SEM images of sodiated carbon gas diffusion layer (GDL) (Na/C) anode and (b) illustration of a full Na–O₂ battery with the sodiated GDL as the anode.^[28] (c) Photographs of corrosion resistant bimetallic Li–Na alloy anode.^[14] Reprinted with permission from ref. 28, 14. Copyright 2015, 2018 Royal Society of Chemistry and Nature Publishing Group.

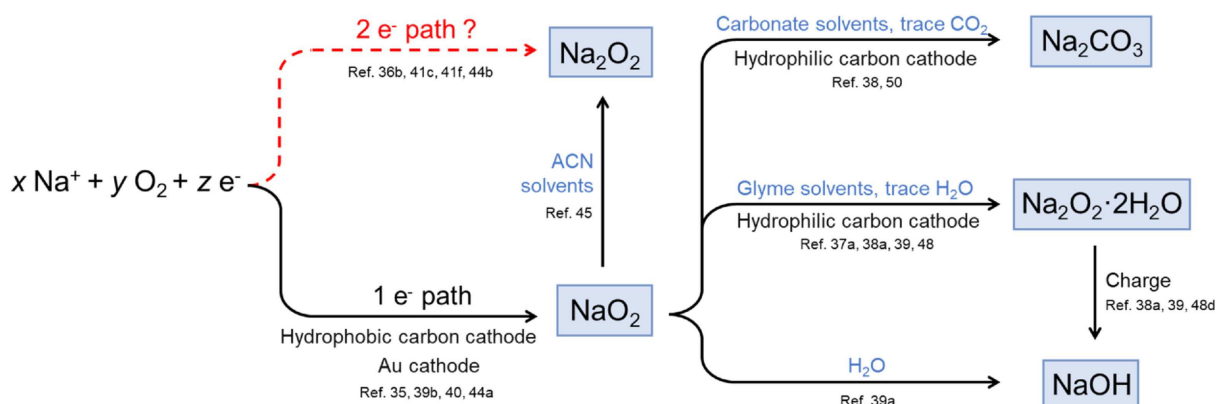


Figure 5. Formation paths for different discharge products in aprotic Na–O₂ batteries. Dashed line indicates evidence for such electrochemical path of 2e[−] is insufficient.

able to believe that NaO_2 is the principle discharge product in ether-based electrolyte such as DME,^[40] dithylene glycol dimethyl ether (DEGDME)^[35] and tetraethylene glycol dimethyl ether (TEGDME).^[39b]

Na_2O_2 has also been identified as the discharge products in ether-based electrolytes by XRD, Raman, selected area electron diffraction (SAED), fourier-transform infrared spectroscopy (FTIR), etc.^[36,38b,41] However, the quality of XRD and Raman is too low to unequivocally confirm that Na_2O_2 is the major discharge product. Evidence from SAED and FTIR is not sufficient to identify the major phase of discharge products as discussed by Bender *et al.*^[42] Recently, Schröder *et al.* tried three approaches to generate Na_2O_2 in ether-based $\text{Na}-\text{O}_2$ batteries.^[43] i) reducing pre-loaded NaO_2 to Na_2O_2 in Ar atmosphere, ii) using Na_2O_2 coated cathode to guide formation of Na_2O_2 in the discharge process, and iii) using dissolved Na_2O_2 to precipitate Na_2O_2 upon discharge. All these approaches yield NaO_2 as the sole discharge product, and they conclude that it is not be possible to electrochemically produce Na_2O_2 in ether-based $\text{Na}-\text{O}_2$ batteries. Nevertheless, other studies indicate that Na_2O_2 can be electrochemically generated on Au disk electrode at substantially low potential (~ 1.5 V vs. Na/Na^+) in DMSO-based electrolyte, which is attributed to the high O_2 affinity of Au electrode.^[44] In a low donor number (DN) solvent such as acetonitrile (ACN), Na_2O_2 can be produced due to disproportionation of NaO_2 .^[45] Using catalyst-loaded cathode or nitrogen-doped carbon as cathode, Na_2O_2 is generated as identified by better XRD and Raman.^[36,41c, f] Until now, there is no consensus on formation of Na_2O_2 in ether-based $\text{Na}-\text{O}_2$ batteries. The difficulties to understand Na_2O_2 formation originate from its low crystallinity, low content, or the complicated composition of discharge products.

In this regard, we try to unveil the possible reasons for the contradictory results reported on Na_2O_2 . In ether-based electrolytes and using hydrophobic carbon cathode without catalysts, the detection of Na_2O_2 is unlikely.^[46] However, using cathode with high affinity to O_2 , such as Au electrode in high DN solvent of DMSO, Na_2O_2 may be electrochemically generated at substantially low potential (~ 1.5 V vs. Na/Na^+).^[44] It is also possible to generate Na_2O_2 in low DN solvent of ACN by disproportionation of NaO_2 .^[45] Alternatively, when catalyst-loaded cathode or nitrogen-doped carbon is employed,^[36,41c,f] Na_2O_2 may be electrochemically produced following a surface-growth path and competing against the formation of NaO_2 via a solution-precipitation path.^[47] At the same time, NaO_2 can also degrade into $\text{Na}_2\text{O}_2 \cdot 2\text{H}_2\text{O}$ or NaOH ,^[39a] making the complicated composition of discharge products.

$\text{Na}_2\text{O}_2 \cdot 2\text{H}_2\text{O}$ has been detected as the principle discharge products in ether-based $\text{Na}-\text{O}_2$ batteries by XRD and O_2 pressure monitoring.^[37a,38a, 39, 48] Recent research indicates that $\text{Na}_2\text{O}_2 \cdot 2\text{H}_2\text{O}$ is possibly originated from NaO_2 , which is initially generated in ether-based $\text{Na}-\text{O}_2$ batteries and undergoes decomposition to $\text{Na}_2\text{O}_2 \cdot 2\text{H}_2\text{O}$. As shown in Figure 5, the key factor that drives the conversion of NaO_2 into $\text{Na}_2\text{O}_2 \cdot 2\text{H}_2\text{O}$ is water, which can be introduced from feeding gas,^[39,48e] electrolyte,^[39a,48c] and leakage of the test setup^[37a] and characterization holder.^[49] Controlled production of $\text{Na}_2\text{O}_2 \cdot 2\text{H}_2\text{O}$ in

aprotic $\text{Na}-\text{O}_2$ batteries has been demonstrated by introducing 10 vol% water into electrolyte or by using wet O_2 .^[39a] In another study, by adding 5000 ppm H_2O to electrolyte, the discharge products with capacity of 2 mAh/cm² are mainly composed of $\text{Na}_2\text{O}_2 \cdot 2\text{H}_2\text{O}$ and CH_3COONa .^[48c] Nevertheless, some contradictory results are also reported. For example, when 6000 ppm and 4000 ppm of H_2O are added to electrolyte, respectively, NaO_2 is still the major discharge product.^[37a,49] By using dynamic high purity O_2 , only $\text{Na}_2\text{O}_2 \cdot 2\text{H}_2\text{O}$ is identified by XRD, while batteries using static O_2 only produce NaO_2 .^[39b] Moreover, when discharged electrode containing NaO_2 is exposed to flowing O_2 for 1 hour, $\text{Na}_2\text{O}_2 \cdot 2\text{H}_2\text{O}$ immediately appears as identified by XRD. In comparation, NaO_2 that does not experience flowing O_2 can be stored in a vacuum pouch for 110 days with a very slow decomposition rate, and no $\text{Na}_2\text{O}_2 \cdot 2\text{H}_2\text{O}$ is detected.^[48e] Stainless steel and glass testing setup generate NaO_2 and $\text{Na}_2\text{O}_2 \cdot 2\text{H}_2\text{O}$ as the major discharge product, respectively. Poor seal of glass testing setup is likely the reason for $\text{Na}_2\text{O}_2 \cdot 2\text{H}_2\text{O}$ formation.^[37a] Furthermore, the transition from pure NaO_2 to $\text{Na}_2\text{O}_2 \cdot 2\text{H}_2\text{O}$ in sealed XRD holder is observed within 3 hours, indicating the leakage of XRD holder and high reactivity of NaO_2 with gas phase water.^[49] Attack of hydrophilic carbon cathode by O_2^- produces $\text{Na}_2\text{O}_2 \cdot 2\text{H}_2\text{O}$ and Na_2CO_3 .^[48a] H-abstraction of diglyme solvent by O_2^- is a possible way for $\text{Na}_2\text{O}_2 \cdot 2\text{H}_2\text{O}$ formation.^[48b]

The presence of NaOH is always paired with $\text{Na}_2\text{O}_2 \cdot 2\text{H}_2\text{O}$, probably due to the side reaction between NaO_2 and water, or due to the conversion of $\text{Na}_2\text{O}_2 \cdot 2\text{H}_2\text{O}$ into NaOH upon charge by the equation of $\text{Na}_2\text{O}_2 \cdot 2\text{H}_2\text{O} \rightarrow 2\text{NaOH} + \text{H}_2\text{O}_2$.^[37a,38a,39,48d] Na_2CO_3 is now widely recognized as the principal discharge product along with Na_2O_2 in carbonate-based electrolyte because of the instability of carbonate solvent towards superoxide radicals.^[38,50]

Discharge products, including NaO_2 , Na_2O_2 , $\text{Na}_2\text{O}_2 \cdot 2\text{H}_2\text{O}$, NaOH and Na_2CO_3 , have significantly different electrochemical properties. Study on their properties provides a mean to accurately quantify the product composition. Constant-current discharge-charge measurement is facile and versatile to determine discharge products. As shown in Figure 6a, NaO_2 has type 1B voltage profiles, showing flat voltage plateaus for both discharge and charge processes with a very low overpotential (< 200 mV).^[35,51] The beginning of charge is accompanied by a voltage spike and the finish is indicated by steep increase of voltage. The voltage profiles for Na_2O_2 reported so far are ambiguous, primarily including type 2 C and 3 C.^[36,41a-d,f,42,51] Until now, there is no consensus on the voltage profiles of Na_2O_2 . Voltage profile of commercial Na_2O_2 with size of 1–5 μm has been reported.^[43] As displayed in Figure 6b, the charge plateau is 3.6 V vs. Na/Na^+ with an initial increase to 4.0 V. At the end of charge, battery potential rose rapidly, indicating decomposition complete of Na_2O_2 . Using CaMnO_3 as catalysts, the electrochemically produced Na_2O_2 shows two voltage plateaus at 2.8 and 3.6 V (Figure 6c).^[36b,41c,f] The voltage plateau at ~ 2.8 V vs. Na/Na^+ can originate from the degradation of simultaneously produced NaO_2 , which degrades into $\text{Na}_2\text{O}_2 \cdot 2\text{H}_2\text{O}$ and NaOH .^[39a] NaOH can be further oxidized with plateaus at 2.7 and 3.1 V vs. Na/Na^+ , depending on the state of

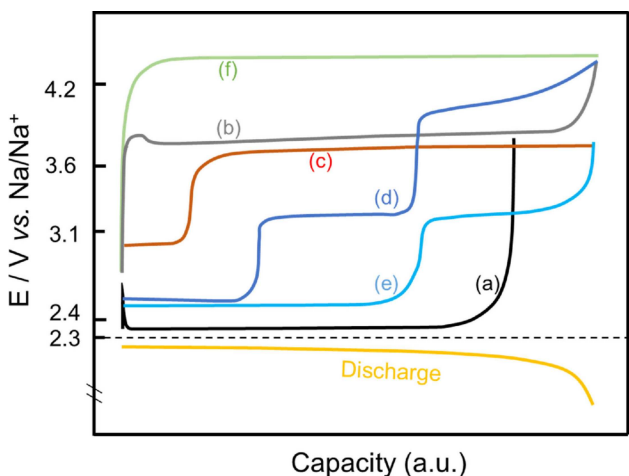
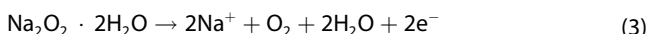


Figure 6. Schematic voltage profiles for different discharge products in aprotic $\text{Na}-\text{O}_2$ batteries, the diagram is recreated according to relevant literature. (a) NaO_2 , battery composition is $\text{Na}/0.5 \text{ M NaOTf-G2/GDL}$,^[35] (b) Commercial NaO_2 , battery composition is $\text{Na}/0.5 \text{ M NaOTf-G2}/\text{Commercial NaO}_2$, the battery is directly charged without initial discharge,^[43] (c) Na_2O_2 , battery composition is $\text{Na}/1 \text{ M NaOTf-G4/CaMnO}_3$ -carbon, the cathode is composed of CaMnO_3 :Super-P:PVdF = 3:6:1 (weight ratio),^[36b] (d) $\text{Na}_2\text{O}_2 \cdot 2\text{H}_2\text{O}$, battery composition is $\text{Na}/\text{NaOTf-G4/GDL}$,^[39a] (e) NaOH , battery composition is $\text{Na}/0.5 \text{ M NaOTf-G4/CNT}$,^[39b] (f) Na_2CO_3 , battery composition is $\text{Na}/1 \text{ M NaClO}_4$ -PC/Ketjen Black C.^[38a] Every discharge product is identified at least by XRD to be the dominant phase, except for (e) where only $\text{Na}_2\text{O}_2 \cdot 2\text{H}_2\text{O}$ is identified but converted into NaOH when charged above $\sim 2.5 \text{ V}$.

NaOH .^[39b] $\text{Na}_2\text{O}_2 \cdot 2\text{H}_2\text{O}$ can also be converted into NaOH .^[37a,38a,39,48d] So, the plateau at $\sim 2.8 \text{ V}$ can be attributed to oxidation of NaOH .

In Figure 6d with a carbon cathode in ether-based $\text{Na}-\text{O}_2$ batteries, the discharge product $\text{Na}_2\text{O}_2 \cdot 2\text{H}_2\text{O}$ shows three different plateaus at ~ 2.4 , ~ 3.2 , and an upper one between 3.5 and 4.3 V vs. Na/Na^+ .^[37a,38a, 39, 48b, d] The plateau at $\sim 3.2 \text{ V}$ is attributed to NaOH because $\text{Na}_2\text{O}_2 \cdot 2\text{H}_2\text{O}$ can be converted into NaOH upon charge.^[38a,39b,48d] The plateau (with certain slope) between 3.5 and 4.3 V is likely related to the oxidation of Na_2O_2 and Na_2CO_3 , because Na_2O_2 and Na_2CO_3 have an apparent charge plateau at $\sim 3.6 \text{ V}$ and 4.2 V , respectively.^[38,46] The plateau at $\sim 2.4 \text{ V}$ was previously assigned to the reaction $\text{Na}_2\text{O}_2 \cdot 2\text{H}_2\text{O} \rightarrow 2\text{NaOH} + \text{H}_2\text{O} + 1/2\text{O}_2$, because the phase change from $\text{Na}_2\text{O}_2 \cdot 2\text{H}_2\text{O}$ to NaOH is observed by XRD when the battery is charged during the 2.4 V plateau.^[38a,39b,48d] However, there is no electron transfer at cathode for the conversion of $\text{Na}_2\text{O}_2 \cdot 2\text{H}_2\text{O}$ into NaOH upon charge, meaning that no plateau will be observed for such reaction.^[39a] Recently, Pinedo *et al.* intentionally produced $\text{Na}_2\text{O}_2 \cdot 2\text{H}_2\text{O}$ in ether-based $\text{Na}-\text{O}_2$ batteries, during which the pressure variation was measured to assess the ratio of electrons to the consumed (or generated) O_2 . During discharge, two-electron transfer is observed for the formation of $\text{Na}_2\text{O}_2 \cdot 2\text{H}_2\text{O}$. Upon charge, the capacity corresponding to the 2.4 V plateau indicates one-electron transfer, implying that $\text{NaO}_2 \rightarrow \text{Na}^+ + \text{O}_2^- + \text{e}^-$ may be involved. However, no XRD signal for NaO_2 is observed, and the gas evolved at the 2.4 V plateau period accounts for 80% of the total consumed gases during discharge, so the 2.4 V plateau is not from the

decomposition of NaO_2 . Instead, it is proposed that the one-electron transfer is due to two parallel reactions simultaneously happened at both the cathode and anode:



To better reveal the plateau at 2.4 V , more carefully designed experiments are needed.

3.2. Choices of Cathode Materials

Cathode materials have significant influence on discharge products of $\text{Na}-\text{O}_2$ batteries. Carbon-based materials are the most commonly investigated cathodes, and their functional groups and specific surface area (SSA) play an important role in discharge process. In addition, catalysts-loaded carbons demonstrate alternative routes to form Na_2O_2 , and lower Na_2O_2 oxidation overpotential. On the other hand, noble metals such as Au that have high affinity to O_2 can alter the morphology and possibly final discharge products. We will discuss in detail how the choice of cathode will affect the performance of $\text{Na}-\text{O}_2$ system.

The amounts of functional groups on cathode have a dramatic influence on discharge products in aprotic $\text{Na}-\text{O}_2$ batteries. Yadegari *et al.* reported that hydrophilic carbon can shift the solution-precipitation process to surface-growth process by promoting the reaction between superoxide and functional groups on carbon surface. By employing hydrophilic carbon cathode, much smaller discharge capacity ($\sim 0.2 \text{ mAh/cm}^2$) is obtained than that of hydrophobic ($\sim 1.2 \text{ mAh/cm}^2$), and the primary discharge products of the hydrophilic carbon are Na_2CO_3 , $\text{Na}_2\text{O}_2 \cdot 2\text{H}_2\text{O}$ and H_2O_2 , instead of NaO_2 . Moreover, nanosized particles are observed on hydrophilic electrode (Table 2c),^[48a] instead of large cubic crystals (Table 2a).

SSA has substantial influence on discharge of $\text{Na}-\text{O}_2$ batteries. Bender *et al.* utilized carbons with surface areas ranging from $1 \text{ m}^2 \text{ g}^{-1}$ to $1500 \text{ m}^2 \text{ g}^{-1}$ to reveal their impact on capacities and morphologies of the discharge products.^[52] NaO_2 is identified to be the only discharge product. The Coulombic efficiency for different carbons in the first cycle varies quite a lot. The lower Coulombic efficiency is probably resulted from the larger amounts of functional groups. Moreover, various morphologies of NaO_2 , such as cubes, films and small particles, are formed on different carbons. The intensity of the spike at initial charge (Figure 6a), which is a typical feature for NaO_2 , is found to depend on SSA of these carbons: the lower the SSA is, the more obvious the spike appears.

The interaction between O_2 and cathode significantly changes the morphology of NaO_2 . Lutz *et al.* proposed that surface energy and O_2/O_2^- affinity of cathode in $\text{Na}-\text{O}_2$ batteries greatly affect the morphology of discharge products. The nucleation rate of NaO_2 on Au electrode is faster than that on Carbon electrode. The fast nucleation rate on Au surface and strong interaction between Au and O_2^- can lead to

Table 2. Cathode effects on the discharge products in aprotic Na–O₂ batteries. (a) Pristine Gas Diffusion Layer (GDL) (Freudenberg H2315),^[37a] (b) Au-coated GDL,^[44a] (c) Oxidized GDL,^[48a] (d) CaMnO₃ cathode, which is composed of CaMnO₃:Super-P:PVDF = 3:6:1 (weight ratio).^[36b] Reprinted with permission from ref. 37a, 44a, 48a, 36b. Copyright 2015, 2017, 2018 Wiley-VCH Verlag GmbH & Co. KGaA American Chemical Society and Royal Society of Chemistry.

| Cathode types | Hydrophobic carbon | Au-coated carbon | Hydrophilic carbon | Catalyst@carbon |
|--------------------------|--------------------|------------------|---|--------------------------------|
| Morphologies | (a) | (b) | (c) | (d) |
| Major discharge products | NaO ₂ | NaO ₂ | Na ₂ CO ₃ , Na ₂ O ₂ ·2H ₂ O, etc. | Na ₂ O ₂ |

formation of thin flakes of NaO₂ with ~3 μm in thickness (Table 2b).^[44a] On the contrary, slow nucleation rate on hydrophobic carbon leads to large cubes of NaO₂ of 10 μm (Table 2a).^[37a] The strong affinity between O₂⁻ and Au electrode is also illustrated by surface enhanced Raman spectroscopy (SERs) experiments. NaO₂ is firstly coated on Au disk electrode, and the SERs signals of O₂⁻ and NaO₂ are monitored. Initially, only NaO₂ signal appears and quickly disappears within ca. 10 mins, and O₂⁻ signal starts to appear and last for long time like 5 hours, implying that O₂⁻ has a strong interaction with Au electrode.^[53]

The catalysts may promote formation of Na₂O₂ (1605 Wh/kg) and reduce its oxidation overpotentials. Cathodes loaded with NiCo₂O₄,^[41c] CaMnO₃,^[36b] Co₃O₄,^[41g,54] RuO₂,^[41e] MnCo₂O₄,^[55] CoB^[41f] and N-doped carbon^[36a,41d] have been investigated. RuO₂ shows high catalytic activity in terms of small charge overpotentials. At of 50 uA/cm², the charge potential remains lower than 3 V for all the discharge capacity, and the battery can be cycled for 100 times with a cut-off capacity of 0.5 mAh/cm². For the cathode without RuO₂, the charge potential is higher than 3 V for ~60% of the discharge capacity. The enhanced catalytic activity of RuO₂ is attributed to the high O₂ affinity with RuO₂.^[41e] Metallic CoB nanosheets also catalyze formation of Na₂O₂ in ether-based Na–O₂ batteries, as indicated by XRD and Raman, and facilitate oxidation of the discharge products.^[41f]

3.3. Amphibian Feature of NaO₂

3.3.1. Mechanism

NaO₂ is the origin of various discharge products in aprotic Na–O₂ batteries, and has a very prominent advantage of low charge overpotentials of <200 mV.^[35] Understanding its formation mechanism is of great importance not only further improving battery performance but also promoting oxygen reduction chemistry. Two different paths have been proposed to explain the formation of NaO₂, as shown in Figure 7, the solution-precipitation and surface-growth path.^[47,56] The surface-growth path illustrates that O₂ is reduced on the cathode surface to generate O₂⁻, which then combines with Na⁺ from the solution and forms a thin layer of NaO₂ on cathode surface. The thickness of NaO₂ layer increases with reduction of O₂ on NaO₂.^[35,47,56] The solution-precipitation path also involves initial reduction of O₂ on the cathode surface, but the reduced O₂ (O₂⁻) dissolves into the electrolyte afterwards.^[47,57] If the reduction rate is faster than the dissolution rate of O₂⁻, a thin layer of NaO₂ will be produced on cathode surface; otherwise, the dissolved O₂⁻ will precipitate on cathode surface or separator when reaching supersaturation.^[57b] Such a dissolution-precipitation process can lead to large NaO₂ cubes or

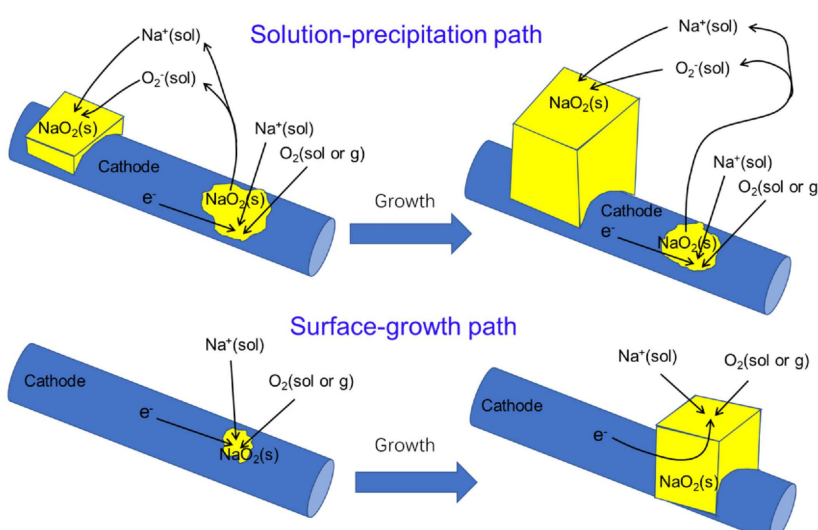


Figure 7. Formation paths for NaO₂ via the solution-precipitation and surface-growth process.

Polyhedrons, offering larger capacities than the surface-growth path.^[58]

A lot of researches have indicated that NaO_2 is formed through the solution-precipitation path.^[47,57] A rotating ring-disk electrode (RRDE) is able to detect dissolved species by measuring ring current, and the substantial solubility of NaO_2 can produce a large ring current.^[40,58] A three-electrode system (Figure 8a), which consists of two carbon cathodes (WE1 and WE2) and one Na anode (CE and RE are the same Na anode), has unambiguously proved that NaO_2 can be generated at one carbon cathode and be oxidized at another carbon cathode, without electrical contacts between these two carbon electrodes. This clearly shows the transport of dissolved O_2^- from WE1 to WE2.^[47] Moreover, operando environmental transmission electron microscopy (TEM) reveals the solution-precipitation path for NaO_2 formation. At discharge, there is no NaO_2 nuclei observed within first 5 seconds, indicating that the initially produced NaO_2 are dissolved. After this initial period, small NaO_2 nuclei starts to form and grow into cubic morphology.^[57a] Atomic force microscope (AFM) on highly oriented pyrolytic graphite (HOPG) shows NaO_2 dissolution and recrystallization during discharge in ether-based electrolyte.^[59] The large amount of NaO_2 cubes observed on separator also implies solution path for the formation of NaO_2 .^[47] Electron paramagnetic resonance (EPR) signals of O_2^- are detected when discharged electrode is immersed in fresh solvent, also implying substantial solubility of NaO_2 .^[48b]

3.3.2. Effects of Solvents

Solvent has a profound influence on the discharge products in aprotic $\text{Na}-\text{O}_2$ batteries. Several different solvents, including ether-based,^[35,38c,40] carbonate-based,^[38] DMSO-based,^[45,53,60] ACN-based^[45] and ionic liquids (ILs),^[38c,61] have been investigated. Ether-based, DMSO-based solvents and ILs favor the formation of NaO_2 as the major discharge product, but the

carbonate-based solvent is unstable and ACN generates only Na_2O_2 .^[34,45a]

DN of solvents in Figure 9 affects the discharge products in the $\text{Na}-\text{O}_2$ batteries. DN is a qualitative measure of Lewis basicity and reflects the capability of a solvent to solvate cations or Lewis acids. For example, S and Na^+ are applied to represent solvent and cation, respectively. Solvation of Na^+ by S is presented by electron donation of S to Na^+ : the stronger the donation, the higher the solvation effect. Solvation of Na^+ modifies its Lewis acidity and changes the discharge products in $\text{Na}-\text{O}_2$ batteries.^[6]

According to hard soft acids bases theory (HSAB), soft acids react faster and bonds stronger with soft bases, whereas hard acids tend to react faster and bonds stronger with hard bases. As shown in Figure 9, Na^+ is classified as hard acid that is more likely to react and have a strong interaction with hard bases like O_2^{2-} , instead of O_2^- that is classified as soft base.^[34,61] This implies that the electrochemically generated O_2^- in low DN solvent, which cannot solvate Na^+ well, is prone to disproportion into O_2^{2-} or O^{2-} in order to pair with hard Lewis acid Na^+ . ACN has a low DN, and thus the electrochemically generated O_2^- immediately disproportionates into O_2^{2-} , producing Na_2O_2 as the final discharge product.^[6,34,45a] On the contrary, solvent with high DN can solvate Na^+ well and making it a soft Lewis acid, thus stabilizing soft Lewis base O_2^- in the electrolyte. Ethers and DMSO have relatively high DN, and they are able to solvate Na^+ ^[6,34,45a] and favor stable and dissolved NaO_2 in the electrolyte. The dissolved NaO_2 precipitates again on cathode surface or separator after reaching supersaturation.

Protons play an essential role in regulating the operation mechanism in gylme-based $\text{Na}-\text{O}_2$ batteries. Xia *et al.*^[48c,58] demonstrates that, in the absence of protons, NaO_2 thin films covering cathode surface are formed and the discharge capacity is negligible. In contrast, the addition of trace amount of water (~ 8 ppm) into the electrolyte results in a dramatic increase in capacity and cubes of NaO_2 of $10 \mu\text{m}$. Further increase of water content leads to an even larger capacity and

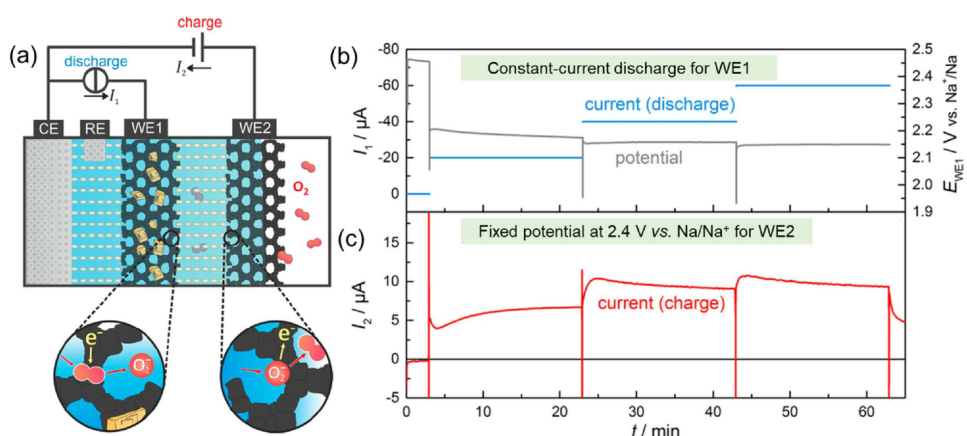


Figure 8. (a) Schematic diagram of a three-electrode system, in which CE and RE are the same and refer to Na metal and WE is the cathode, (b) Voltage profile of WE1, the current is fixed at -20 , -40 and -60 μA for ~ 23 mins, respectively, so that O_2 can be reduced at WE1, (c) Voltage profile of WE2, the potential is fixed at 2.4 V vs. Na/Na^+ so that O_2^- , which is generated on WE1, will be oxidized.^[47] Reprinted with permission from ref. 47. Copyright 2015 American Chemical Society.

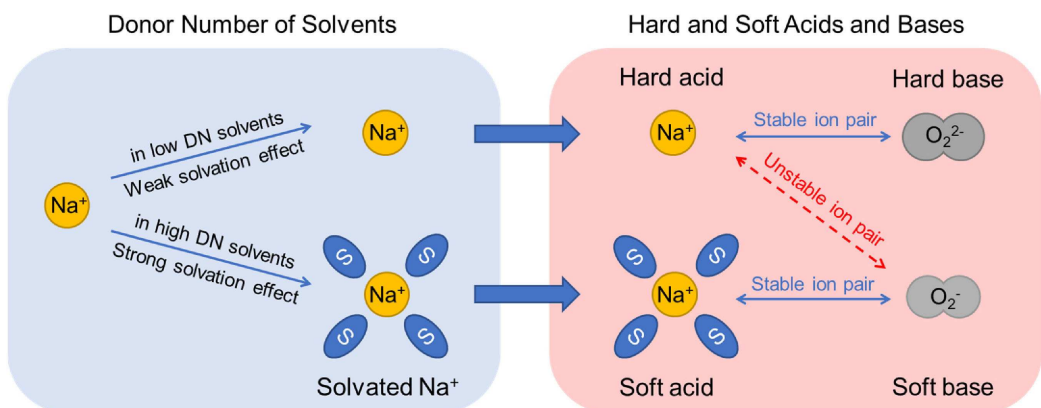


Figure 9. Influence of solvent DN on discharge products in aprotic $\text{Na}-\text{O}_2$ batteries. High DN solvent can make hard Lewis acid Na^+ soft, which then forms stable pair with soft Lewis base O_2^- . Low DN solvent does not change softness of Na^+ , which cannot form stable pair with O_2^- . Consequently, O_2^- will decompose into hard Lewis base O_2^{2-} , and then form stable pair with Na^+ .^[6,34]

NaO_2 cubes. The mechanism is proposed by Xia *et al.*^[58] as follows:



Where, HA represents a weak acid that can easily release protons. The electrochemically produced O_2^- abstracts a proton from HA and forms HO_2 as shown in Equation 5. The driving force toward NaO_2 in Equation 6 is the large Gibbs free energy related to the formation of NaO_2 ($\Delta G = -437.5 \text{ kJ mol}^{-1}$).

3.3.3. Effects of Pressure and Current Density

O_2 pressure^[62] and current density^[49,57b,62a,63] influence the distribution and particle size of NaO_2 in aprotic $\text{Na}-\text{O}_2$ batteries. The O_2 concentration in the electrolyte is directly related to its partial pressure in gas phase. Hartmann *et al.* reveals that the O_2 concentration in ether-based solvent linearly increases with its partial pressure.^[62b] It accordingly leads to increase of the discharge capacity. O_2 pressure not only affects the discharge capacity but also changes the distribution of NaO_2 on cathodes. At low O_2 pressure, NaO_2 is preferentially precipitated on the O_2 reservoir side of the cathode, while at high O_2 pressure it tends to be homogeneously distributed along the thickness of cathode.^[62a] If O_2 pressure is low during discharge process, O_2 near separator will be depleted quickly, and then the areas of cathode facing separator will become inactive for O_2 reduction. On the contrary, at high O_2 pressure, O_2 in the electrolyte is always enough to the reduction, contributing to a more uniform distribution of NaO_2 .

Current density has significant influence on the NaO_2 size and its particle size distribution.^[49,57b,62a,63] High current density

favors small size of NaO_2 , probably due to the increased amounts of nuclei sites.^[57b,63] The particle size is not uniform along the cathode thickness, specifically from the O_2 reservoir side to the separator side. Larger particles are found on O_2 reservoir side, and such size difference is more profound at lower current density.^[63] Simultaneously, more NaO_2 particles are found on O_2 reservoir side, and the distribution difference increases at larger current density.^[62a] This is because no sufficient O_2 is provided at the cathode near separator at high current densities.^[49,63]

4. Electrolytes

4.1. Solvents

In an extremely rough environment in $\text{Na}-\text{O}_2$ batteries, solvents are faced with the highly oxidative oxygen, superoxide and discharge products, as well as the reductive and reactive sodium anode. The chemical stability of solvents determines the cycling performance. Decomposition of solvents usually results in side product at the cathode and continuous consumption of electrolyte and sodium anode, inducing high charging overpotential and the short cycle life. Besides, solvent molecules in $\text{Na}-\text{O}_2$ batteries coordinate with the sodium ion, salt anions and superoxide.^[6,40,64] The interaction among solvent molecules, sodium ions, salt anions and superoxide have a strong impact on the cycling performances and even result in different discharging product of NaO_2 or Na_2O_2 . In the light of the $\text{Li}-\text{O}_2$ batteries, nonaqueous electrolyte of ethers,^[35] ACN,^[6] DMSO etc.^[34] are studied in $\text{Na}-\text{O}_2$ batteries. The chemical stability against nucleophilic attack or H-abstraction reaction and solvents-solute interaction based on different polarities are reported.^[38c,65]

4.1.1. Ethers

After carbonate-based electrolytes were confirmed unstable with superoxide,^[38b,c] ethers were successfully introduced in the Na–O₂ batteries. In 2013, Hartmann *et al.*^[35] used diglyme with sodium triflate salts in the Na–O₂ battery, achieving dominant discharge product of NaO₂ and an unexpected small overpotential (≤ 200 mV). The enhanced performance was attributed to the relative high stability of ethers against highly nucleophilic superoxide anion O₂[−]. Apart from the stability at cathode, ethers are also proven with high stability at sodium metal anode.^[22] With the enhanced stability, ether-based electrolytes, especially glyme-based electrolytes are widely utilized in Na–O₂ batteries, even taking an irreplaceable role in current researches.

Although with enhanced chemical stability, DME-based Li–O₂ batteries was reported with limited O₂ efficiency by McCloskey *et al.*^[66] Comparing with Li–O₂ batteries, Na–O₂ batteries possess cleaner chemistry in ether-based electrolyte. Applying quantitative titrations and differential electrochemical mass spectrometry (DEMS), the yield of the main discharge product of NaO₂ or Li₂O₂ was reported to be 0.945 and 0.91 in ether-based Na–O₂ batteries and Li–O₂ batteries. The ratio of O₂ evolution on charge to O₂ reduction on discharge was calculated to be 0.93 and 0.78 respectively, indicating a better

reversibility of Na–O₂ batteries.^[2] Further, on-line electrochemical mass spectrometry (OEMS) characterization was reported by Black *et al.*^[65] As illustrated in Figure 10a, the integration of O₂ evolved with respect to the total charge below 3.0 V was calculated to be 1.10 e[−]/O₂. The subsequent stepped charging profile was characterized with CO₂ evolution along with trace amount of O₂. By iodometric titration and mass spectrometry in Figure 10b, approximately 10% of the discharge product was a mixture of sodium acetate, sodium formate, methoxy(oxo) acetic anhydride and Na₂CO₃, which were originated from decomposition of ether solvents in the discharging process. Only a small amount of Na₂¹³CO₃ (<1%) was originated from ¹³C-labelled carbon cathode in charging processes. Unlike the decomposition of organic carbonates, ethers were suggested to suffer from H-abstraction by the highly nucleophilic O₂[−] species. The decomposition mechanism of glyme was suggested in Figure 10c. Besides, NaO₂ is also reported to induce the decomposition. In 2018, Yadegari *et al.*^[67] used Raman imaging technique to evaluate the stability of NaO₂ on a dry air cathode or with additional electrolyte, indicating that the decomposing of NaO₂ is much faster with DEGDME electrolyte. A decomposition pathway was proposed based on H-abstraction reaction from NaO₂. However, given that NaO₂ is soluble and possibly generates O₂[−] in solvents, whether H-abstraction reaction is induced by NaO₂ or O₂[−] is unclear. Computational

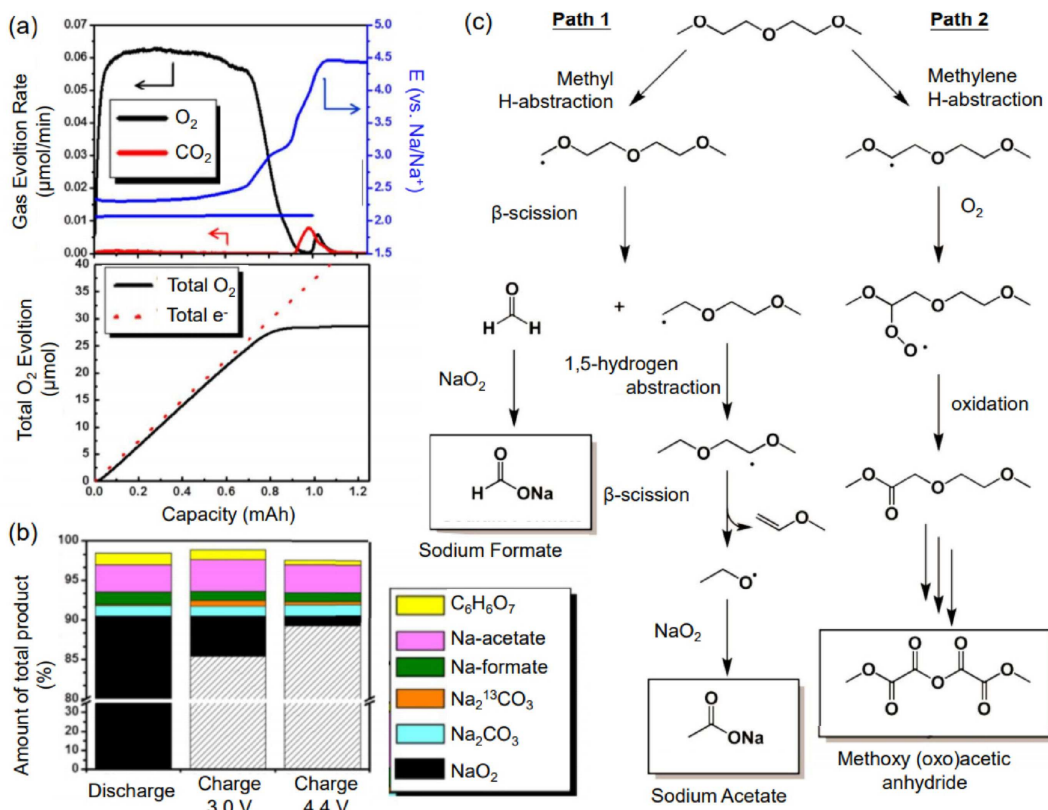


Figure 10. (a) Discharge/charge curve for a Na–O₂ battery with a ¹³C cathode, corresponding O₂ and CO₂ evolution profiles and the integrated values of oxygen evolution (black solid line) compared to theoretical O₂ evolution (dashed red line). (b) Products as a fraction of the total theoretical product at different stages of battery operation. (c) Proposed reaction pathways for DEGDME in Na–O₂ batteries.^[65] Reprinted with permission from ref. 65. Copyright 2016 Wiley-VCH Verlag GmbH & Co. KGaA.

calculation on the stability of crystal NaO_2 is suggested, as attempted in stability evaluation on Li_2O_2 clusters.^[68]

Glymes with different chain length, including DME, DEGDME, triethylene glycol dimethyl ether (TRIDME), TEGDME and polyethylene glycol dimethyl ether (PEGDME) are extensively investigated in $\text{Na}-\text{O}_2$ batteries.^[4b,48e,64,69] The solvent-solute association among different glymes can lead to distinguish battery performances. Recently, using molecular dynamics simulations, Kumar *et al.*^[64] reported detailed descriptions of the solvation structures for NaOTf in different glymes (from DME to TEGDME). The simulations showed that Na^+ in glymes was coordinated by 6 to 7 oxygens, contributed from glyme molecules and/or OTf^- . In the solvation shell of Na^+ , various solvation structures were observed, including Na^+ coordinated only by glyme molecules, Na^+ associated with glyme molecules and one triflate anion or more. In short chain glymes of DME or diglyme, Na^+ tended to coordinate with both triflate anions and glyme solvents. As for long chain glymes of TRIDME or TEGDME, the first solvation shell was occupied mostly by solvent molecules with much less anticipation of anions. The impact of solvation effect of different glymes (DME, DEGDME and TEGDME) on battery performances was reported by Lutz *et al.*^[40] The chelation effect was enhanced with increasing chain length, resulting in more dissolved NaO_2 . Interestingly, DME solvent with negligible dissolved NaO_2 exhibited the highest discharge capacity with the largest cubic crystals, which was attributed to the lowest desolvation barrier. The strong Na^+ chelation of TEGDME led to solvent-separated ions of Na^+ and O_2^- , which was resulted from the increased activation barrier for desolvation. The understanding of solvation structures in electrolyte is important to determine the electrolyte effect on the discharge product. More works are recommended to clarify the causal relationship between different solvation structure and resultant discharging performances.

4.1.2. DMSO and ACN

Apart from carbonates and ethers, DMSO and ACN are also investigated in the $\text{Na}-\text{O}_2$ batteries.^[6,34] Although due to the reaction of DMSO and Na and the high vapor pressure of ACN, their applications in $\text{Na}-\text{O}_2$ batteries are limited, yet the researches in DMSO-, ACN-based electrolyte provide valuable understanding on the association between electrolyte properties and battery chemistry. DMSO with both high DN (29.8) and AN (19.3) and ACN with low DN (14.1) but high AN (18.9) are perfect examples for the solvation interaction investigation.^[70] In 2017, Lutz and co-workers^[6] demonstrated the chemical environment of Na^+ in different solvents. With ^{23}Na -NMR visualization, solvent-solute interaction was illustrated as shown in Figure 11a. They demonstrated the solvation effect on the ion paring structure. As illustrated in Figure 11a, in a weak solvating DME solvent, the Na^+ and anions favor contact ion pairs, where the $^{23}\text{Na}^+$ chemical shifting is strongly influenced by the anions. As for ACN with low DN but high AN, solvation of anions restricted the anion influence, resulting in separated ions structure. However, in DMSO, high DN and AN determined the strong anions and cations association capability, the Na^+ and anions are separated by solvents and the Na^+ chemical shifting did not change with the different anions. Besides, the impact on NaO_2 stability from solvent/anion pairs was reported by Dilimon *et al* (as shown in Figure 11b).^[34] The NaO_2 stability was valued by the standard rate constant (k_o) of oxygen/superoxide electrochemistry, red color refers to higher k_o . As illustrated in the diagram, the NaO_2 stability or reversibility of oxygen/superoxide electrochemistry increases in high-DN pairs of anion/solvent (e.g., OTf^-/DMSO). In OTf^-/DMSO or $\text{ClO}_4^-/\text{DMSO}$, superoxide formed at the first step oxygen reduction reaction (ORR) process, formation of Na_2O_2 only occurred in the second step ORR. However, in $\text{PF}_6^-/\text{DMSO}$, superoxide immediately disproportionated into peroxide, resulting in Na_2O_2 as the discharge product.

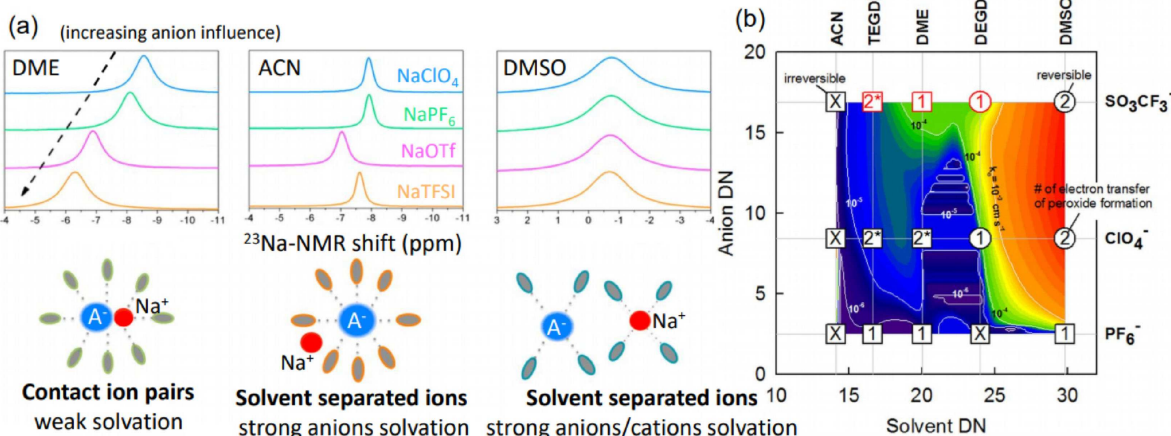


Figure 11. (a) ^{23}Na -NMR visualization of the impact of the ClO_4^- (blue line), PF_6^- (green line), OTf^- (pink line) and bis(trifluoromethylsulfonyl)imide (TFSI^-) (orange line) anion on the Na^+ chemical shift in DME, ACN, and DMSO.^[6] (b) Contour plots of the standard rate constants (k_o) of superoxide formation on 2D DN map for superoxide stability. Gutmann's DN and Linert's DN values were used for solvents and anions, respectively.^[34] Reprinted with permission from ref. 6, 34. Copyright 2017 American Chemical Society and Nature Publishing Group.

4.2. Sodium Salts

Comparing with solvents, the instability of salts towards superoxide is rarely reported. However, anion decompositions at anode are reported. Grimaud *et al.*^[6] evaluated the solid electrolyte interface (SEI) (Figure 12) in presence of different anions (ClO_4^- , PF_6^- , OTf^- or TFSi^-) in DME solvents, which are most commonly used in current researches. The results showed that the PF_6^- anion in combination with DME generated NaF containing SEI, which is sufficiently stable and ionic conductive. Owing to the larger anion of OTf^- or weaker Na–Cl bond generated from ClO_4^- , other SEIs generated by OTf^- and ClO_4^- were unstable. Especially for TFSi^- anion, probably due to its large size, was found to be detrimental to the Na metal anode. However, a conflicting result was published by Shi and co-workers.^[71] They added 0.01 M KTFSi as a bifunctional electrolyte additive in a NaOTf containing TEGDME electrolyte, indicating that the generated SEI with sodium nitride (Na_3N) and oxynitrides (NaN_xO_y). To be noticed, the later experiment was operated in $\text{Na} \parallel \text{Na}$ symmetric batteries without exposure to oxygen atmosphere. Thus, the opposite experiment results may be due to the oxygen involved decomposition, which need further verifications.

In electrolytes, salts anions also have an impact on the discharge products. Instead of Gutmann's DN, Linert's DN is used for anions. As reported by Dilimon *et al.*,^[34] the anions with higher DN led to better stability of superoxide (as shown in Figure 11b). The anions with different DN also have an impact on the crystal size of the discharge product. The anions of PF_6^- with lower DN was reported to generate smaller NaO_2 crystal and lower discharge capacity, and OTf^- with 6–7 times

higher DN led to larger domain size of NaO_2 and higher capacity. It was reported that due to the weak stability of Na–O₂ complex in PF_6^- , the discharge product of NaO_2 covered the cathode at the initial stage of discharge, resulting in the low discharge capacity.^[72]

What's more, the salt concentration has an impact on the battery performance. A recent research showed a strong correlation between the electrolyte salt concentration and the NaO_2 crystal size.^[73] They monitored the NaO_2 crystal size on a glassy carbon electrode with different concentrations of NaOTf in DME, demonstrated that larger crystal sizes are expected at lower salt concentrations. According to the discussion, for much larger amount of Na^+ in electrolyte, the integration of O_2^- was likely rate-determining for NaO_2 crystal growth. With decreasing concentration of sodium salts, more O_2^- , which was not participated in the ion-pairing ($\text{Na}^+, \text{O}_2^-$) was able to increase the growth rate of NaO_2 , resulting in larger crystal size. To obtain favor larger crystal size and simultaneously guarantee a proper salts concentration, they added 0.5 M of 1,4,7,10,13,16-hexaoxacyclooctadecane (18-Crown-6) as an electrolyte additive to weaken ion-pairing association. Crown ethers known with strong coordination with sodium ions were reported to increase the crystal size of NaO_2 , further increase the discharge capacity in a Na–O₂ battery.

4.3. Additives

To promote the performance of Na–O₂ batteries, various of additives have been introduced in the electrolyte. On decreasing the charging overpotential, redox mediators (RMs)

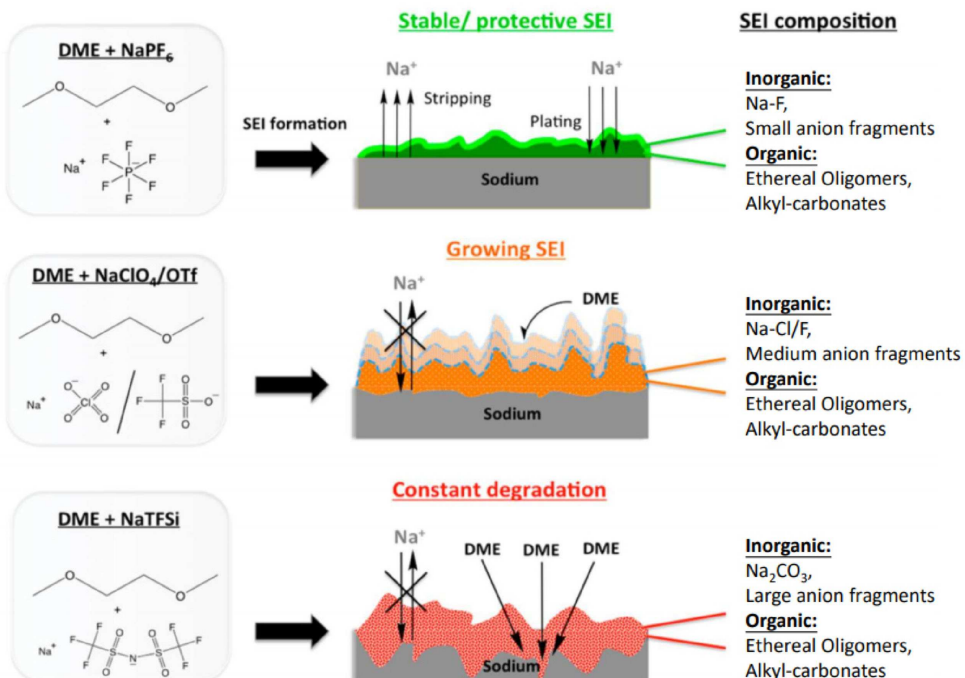


Figure 12. Illustration of the SEI formation mechanism and its composition in different DME electrolytes.^[6] Reprinted with permission from ref. 6. Copyright 2017 American Chemical Society.

are initially introduced in the electrolytes in Li–O₂ batteries.^[74] In the charging process, RMs with higher redox potential are preferentially reduced by electron, and chemically reduce the discharge product subsequently. RMs of NaI (3.2 V vs Na/Na⁺),^[41a] organometallic ferrocene (Fe(C₅H₅)₂) (3.1 V vs Na/Na⁺)^[75] and ethyl viologen (EtV) with the redox pair of EtV⁺/EtV²⁺ (2.3 V vs Na/Na⁺)^[76] were demonstrated in Na–O₂ batteries with enhanced cycling stability. However, due to the better electrochemical reversibility and much lower charging overpotential of NaO₂ than that of Li₂O₂. Whether a redox mediator is needed in a Na–O₂ battery is disputable. Otherwise, phase-transfer catalysis of H₂O^[26,58] and SEI modifying additives,^[27] are discussed in the former section of this review.

4.4. Ionic Liquids

Ionic liquids are a promising candidate for electrolytes in Na–O₂ batteries. They are completely composed of anions and cations, possessing enhanced electrochemical and thermal stability, high ionic conductivity and negligible vapor pressure.^[77] On the other hand, the high viscosity, limited O₂ solubility and diffusivity may restrict the battery performance. However, the chemical stability in the rough battery environment and electrolyte effects on the battery behavior remain unclear.

Currently, phosphonium-,^[78] piperidinium-^[38c] and pyrrolidinium-based^[79] ILs have been demonstrated with potential as electrolytes for metal-air batteries. The chemical structure of the cations in the IL significantly affects the reversible one-electron O₂⁻/O₂ process. Imidazolium-based ILs with positively charged carbon atoms prefer to get attacked by superoxide as reported.^[80] While, pyrrolidinium e.g. [C₄mpyr]⁺, or quaternary ammonium, e.g. [N_{1,1,1,6}]⁺, cations without positively charged carbon atoms are regarded to be stable against superoxide, which are promising for Na–O₂ batteries. In 2017, Azaceta *et al.*^[61] reported oxygen reduction reaction in ionic liquid N-butyl-N-methylpyrrolidinium bis(trifluoromethanesulfonyl)imide (PYR14TFSI) with various concentration of sodium cations. The results indicated the solution-path as well as the surface-path of ORR existed at the low concentration and high concentration electrolyte respectively. Besides, a pyrrolidinium-based ionic liquid, N-butyl-N-methyl pyrrolidinium bis(trifluoromethylsulfonyl)imide ([C₄mpyr][TFSI])^[79b] was demonstrated achieving reversible oxygen reduction reaction. The result indicated that superoxide interacts/reacts preferentially with Na⁺ on increasing the NaTFSI concentration, so that the Na⁺–O₂⁻ paring structure is predominant. Recently, concentrated electrolyte of NaTFSI in [C₄mpyr][TFSI] was used in IL-based Na–O₂ batteries.^[81] The investigation demonstrated that with an increasing concentration of NaTFSI salts, an enlarged discharge capacity, enhanced cyclability and declined overpotential were obtained. The promoted performance was attributed to the enhanced interaction between O₂⁻ and Na⁺ rather than [C₄mpyr]⁺, which lowered the desolvation energy of NaO₂ from the electrolyte.

4.5. Concentrated Electrolytes

Concentrated electrolytes, also known as solvent-in-salt electrolytes, are a novel strategy to stabilize the electrolytes as well as the sodium anode. By using salts or solvents with high solubility, usually TFSI⁻ or FSI⁻-based salts or DMSO solvents, electrolytes with nearly equivalent mole amounts of solvents to salts is obtained. In concentrated electrolyte, solvents are largely coordinated with salts, and the free solvent molecules are decreased, which decay the dissolution of impurities increase the electrolyte stability and suppress the dendrite formation through a dense protective SEI.^[82] Concentrated NaTFSI in DMSO demonstrated high reversibility in Na–O₂ batteries.^[60] The use of DMSO in the Na–O₂ battery is limited due to the reaction between Na and DMSO. With the increasing concentration, the free DMSO molecules were reduced, hence increasing the stability of metallic sodium anode. Moreover, ab initio molecular dynamics indicated that Na(DMSO)₃(TFSI)-like solvation structures existed in the electrolyte environment and demonstrated better thermodynamically stability. However, concentrated strategy may not be adapted to every electrolyte system. In 2018, Na–O₂ batteries with different concentrations of NaTFSI in DME was reported by Tatara *et al.*^[83] The research indicated that decreasing solvation of NaO₂ by less free DME and increasing stabilization of O₂⁻ by more Na⁺ resulted in a volcano-shaped profile for NaO₂ solubility. As the concentration increased, the NaO₂ solubility rose at the first stage, then reduced after reaching to a peak. Thereby, crystal size and discharge capacity were found to be with the same trend. Besides, an increased viscosity and thus decreased ionic conductivity that generated large overpotential in concentrated electrolyte also limited the performances of Na–O₂ batteries.

5. Conclusions and Perspectives

Global efforts to integrate renewable energy and electrify vehicles have led to rapid growth in the battery energy storage market at double-figure rates.^[84] Despite serious challenges, the reversible Na–O₂ battery remains an attractive option of storage battery. It is posed to resolve a fundamental limitation of material supply in the large-scale deployment of its technological relatives, viz. the more developed Li–O₂ battery, and the undeveloped Li–O₂ battery. The use of oxygen in cathode of the Na–O₂ battery substantially increases the overall energy density, but creates vulnerability to irreversible chemistry. The use of a sodium anode, on the other hand, introduces safety issues of dendrites. Recent research indicates promising directions to mitigate these problems.

By proper choice of electrode materials or solvents, electrolytes, sodium deposited during re-charge can be promoted to grow in the lateral direction and hence minimize dendrite formation. The use of bismuth alloy has demonstrated a successful step in this direction and at the same time creates a favorable porous structure for reversible cycling. Similar positive effects can also be shown with electrode surface

modifications and solution additives. Dendrite can also be suppressed mechanically by special separator and current collector. An issue coupled with dendrite is the uniformity and stability of the SEI which appears to be influenced positively by similar materials and operation parameters made to minimize dendrites.

Similar to the Li–O₂ battery with concern of stability arising from redox products of oxygen, the Na–O₂ battery has reaction pathways leading to different oxides. Unlike peroxide as the oxidation product in the Li–O₂ battery, the Na–O₂ battery has superoxide as the more stable and reversible oxidation product which is also more kinetically reversible, leading to a small overpotential. A unique feature of the Na–O₂ battery cathode is the partial solubility and amphibian character of sodium superoxide. This has created problems of degradations in solution e.g. with solvent degradation products of Na₂CO₃, CH₃COONa. But at the same time, it creates an opportunity of more distributed storage of reactions products. E.g. a solution catalyzed solution-precipitation growth transfer process has been observed. Full understanding of the electrochemical and non-electrochemical paths in both solid and solution phases are needed before designing cathode system for reversible NaO₂ formation. The prospect of peroxide as alternative product with higher capacity should not be ruled out as alternative electrolyte and solid-solution environment may enhance its stability. Further research to reveal intermediates and mechanistic details in solution and solid phases are imperative to advance the technology and enable design of cathode materials, electrode structure, electrocatalysts, and possibility homogeneous catalysts/stabilizers in the solution phase. Advanced operando techniques will be particularly powerfully in these studies.

The greatest promise of breakthrough lies in the identification of an optimum solvent-electrolyte-additives system that is compatible to the new chemistry of the Na–O₂ batteries. The solution environment is critical as it impacts different processes at anode and cathode, including dendrite and SEI formation, stability and solubility of NaO₂, and enabling of peroxide pathway. The parameter space is big and early research has already indicated progress, e.g. identifying ethers for enhancing stability of NaO₂, compared to carbonates, DMSO and ACN. Computational techniques such as density functional theories (DFT) can accelerate progress by minimizing experimental efforts. E.g. theories using the DN concept and protons-catalysis have been proposed to explain solution mechanism.

Intensive materials and mechanistic investigations are needed to further develop the Na–O₂ battery technology. The fundamental advantages of theoretical gravimetric energy density and sustainable sodium resource are sound. Several promising directions to improve stability and reversibility are identified with immense research opportunities.

Acknowledgements

We acknowledge the financial support from Ministry of Science and Technology of China (2017YFA0206700) and National Natural Science Foundation of China (NSFC) with grant No. 51761165025 and 51671107; NSFC/Research Grant council (RGC) of Hong Kong Joint Research Scheme N_HKU728/17 and GRF 17300014.

Conflict of Interest

The authors declare no conflict of interest.

Keywords: sodium-oxygen batteries • sodium metal protection • sodium superoxide • solution-precipitation • superoxide crossover

- [1] a) Y. C. Lu, B. M. Gallant, D. G. Kwabi, J. R. Harding, R. R. Mitchell, M. S. Whittingham, Y. Shao-Horn, *Energy Environ. Sci.* **2013**, *6*, 750–768; b) F. Li, J. Chen, *Adv. Energy Mater.* **2017**, *7*, 1602934.
- [2] B. D. McCloskey, J. M. Garcia, A. C. Luntz, *J. Phys. Chem. Lett.* **2014**, *5*, 1230–1235.
- [3] B. Sun, C. Pompe, S. Dongmo, J. Zhang, K. Kretschmer, D. Schröder, J. Janek, G. Wang, *Adv. Mater. Technol.* **2018**, *3*, 1800110.
- [4] a) L. Medenbach, C. L. Bender, R. Haas, B. Mogwitz, C. Pompe, P. Adelhelm, D. Schröder, J. Janek, *Energy Technol.* **2017**, *5*, 2265–2274; b) X. Bi, X. Ren, Z. Huang, M. Yu, E. Kreidler, Y. Wu, *Chem. Commun.* **2015**, *51*, 7665–7668.
- [5] C. Zhao, Y. Lu, J. Yue, D. Pan, Y. Qi, Y. S. Hu, L. Chen, *J. Energy Chem.* **2018**, *27*, 1584–1596.
- [6] L. Lutz, D. Alves Dalla Corte, M. Tang, E. Salager, M. Deschamps, A. Grimaud, L. Johnson, P. G. Bruce, J. M. Tarascon, *Chem. Mater.* **2017**, *29*, 6066–6075.
- [7] R. Dugas, A. Ponrouch, G. Gachot, R. David, M. R. Palacin, J. M. Tarascon, *J. Electrochem. Soc.* **2016**, *163*, A2333–A2339.
- [8] X. Lin, Q. Sun, H. Yadegari, X. Yang, Y. Zhao, C. Wang, J. Liang, A. Koo, R. Li, X. Sun, *Adv. Funct. Mater.* **2018**, *28*, 1801904.
- [9] B. Liu, J. G. Zhang, W. Xu, *Joule* **2018**, *2*, 833–845.
- [10] H. Zhao, N. Deng, J. Yan, W. Kang, J. Ju, Y. Ruan, X. Wang, X. Zhuang, Q. Li, B. Cheng, *Chem. Eng. J.* **2018**, *347*, 343–365.
- [11] N. Xiao, X. Ren, W. D. McCulloch, G. Gourdin, Y. Wu, *Acc. Chem. Res.* **2018**, *51*, 2335–2343.
- [12] a) S. Wei, S. Choudhury, J. Xu, P. Nath, Z. Tu, L. A. Archer, *Adv. Mater.* **2017**, *29*, 1605512; b) Q. Zhang, Y. Lu, L. Miao, Q. Zhao, K. Xia, J. Liang, S. L. Chou, J. Chen, *Angew. Chem. Int. Ed.* **2018**, *57*, 14796–14800.
- [13] Y. Lu, Q. Zhang, M. Han, J. Chen, *Chem. Commun.* **2017**, *53*, 12910–12913.
- [14] J. I. Ma, F. I. Meng, Y. Yu, D. p. Liu, J. m. Yan, Y. Zhang, X. b. Zhang, Q. Jiang, *Nat. Chem.* **2018**, *11*, 64–70.
- [15] S. Choudhury, S. Wei, Y. Ozhabes, D. Gunceler, M. J. Zachman, Z. Tu, J. H. Shin, P. Nath, A. Agrawal, L. F. Kourkoutis, T. A. Arias, L. A. Archer, *Nat. Commun.* **2017**, *8*, 898.
- [16] H. Yang, J. Sun, H. Wang, J. Liang, H. Li, *Chem. Commun.* **2018**, *54*, 4057–4060.
- [17] Q. Zhang, Y. Lu, M. Zhou, J. Liang, Z. Tao, J. Chen, *Inorg. Chem. Front.* **2018**, *5*, 864–869.
- [18] A. Wang, X. Hu, H. Tang, C. Zhang, S. Liu, Y. W. Yang, Q. H. Yang, J. Luo, *Angew. Chem. Int. Ed.* **2017**, *56*, 11921–11926; *Angew. Chem.* **2017**, *129*, 12083–12088.
- [19] S. Liu, S. Tang, X. Zhang, A. Wang, Q.-H. Yang, J. Luo, *Nano Lett.* **2017**, *17*, 5862–5868.
- [20] F. Ding, W. Xu, G. L. Graff, J. Zhang, M. L. Sushko, X. Chen, Y. Shao, M. H. Engelhard, Z. Nie, J. Xiao, X. Liu, P. V. Sushko, J. Liu, J. G. Zhang, *J. Am. Chem. Soc.* **2013**, *135*, 4450–4456.
- [21] Z. Zhu, X. Shi, D. Zhu, L. Wang, K. Lei, F. Li, *Research* **2019**, *2019*, 6180615.
- [22] Z. W. Seh, J. Sun, Y. Sun, Y. Cui, *ACS Cent. Sci.* **2015**, *1*, 449–455.

- [23] J. L. Ma, Y. B. Yin, T. Liu, X. B. Zhang, J. M. Yan, Q. Jiang, *Adv. Funct. Mater.* **2018**, *28*, 1703931.
- [24] C. Monroe, J. Newman, *J. Electrochem. Soc.* **2005**, *152*, A396–A404.
- [25] Y. Ansari, K. Virwani, S. Yahyazadeh, L. E. Thompson, E. Lofano, A. Fong, R. D. Miller, Y.-H. La, *Adv. Energy Mater.* **2018**, *8*, 1802603.
- [26] I. I. Abate, L. E. Thompson, H. C. Kim, N. B. Aetukuri, *J. Phys. Chem. Lett.* **2016**, *7*, 2164–2169.
- [27] S. Wu, Y. Qiao, K. Jiang, Y. He, S. Guo, H. Zhou, *Adv. Funct. Mater.* **2018**, *28*, 1706374.
- [28] C. L. Bender, B. Jache, P. Adelhelm, J. Janek, *J. Mater. Chem. A* **2015**, *3*, 20633–20641.
- [29] W. Wang, W. Li, S. Wang, Z. Miao, H. K. Liu, S. Chou, *J. Mater. Chem. A* **2018**, *6*, 6183–6205.
- [30] H. Hou, C. E. Banks, M. Jing, Y. Zhang, X. Ji, *Adv. Mater.* **2015**, *27*, 7861–7866.
- [31] C. Wang, L. Wang, F. Li, F. Cheng, J. Chen, *Adv. Mater.* **2017**, *29*, 1702212.
- [32] K. Zhang, M. Park, L. Zhou, G. H. Lee, J. Shin, Z. Hu, S. L. Chou, J. Chen, Y. M. Kang, *Angew. Chem. Int. Ed.* **2016**, *55*, 12822–12826; *Angew. Chem.* **2016**, *128*, 13014–13018.
- [33] W. Li, S. L. Chou, J. Z. Wang, J. H. Kim, H. K. Liu, S. X. Dou, *Adv. Mater.* **2014**, *26*, 4037–4042.
- [34] V. S. Dillimon, C. Hwang, Y. G. Cho, J. Yang, H. D. Lim, K. Kang, S. J. Kang, H. K. Song, *Sci. Rep.* **2017**, *7*, 17635.
- [35] P. Hartmann, C. L. Bender, M. Vračar, A. K. Dürr, A. Garsuch, J. Janek, P. Adelhelm, *Nat. Mater.* **2013**, *12*, 228–232.
- [36] a) Y. Li, H. Yadegari, X. Li, M. N. Banis, R. Li, X. Sun, *Chem. Commun.* **2013**, *49*, 11731–11733; b) Y. Hu, X. Han, Q. Zhao, J. Du, F. Cheng, J. Chen, *J. Mater. Chem. A* **2015**, *3*, 3320–3324.
- [37] a) X. Bi, R. Wang, L. Ma, D. Zhang, K. Amine, J. Lu, *Small Methods* **2017**, *1*, 1700102; b) H. Yadegari, Y. Li, M. N. Banis, X. Li, B. Wang, Q. Sun, R. Li, T. K. Sham, X. Cui, X. Sun, *Energy Environ. Sci.* **2014**, *7*, 3747–3757.
- [38] a) J. Kim, H. D. Lim, H. Gwon, K. Kang, *Phys. Chem. Chem. Phys.* **2013**, *15*, 3623–3629; b) Q. Sun, Y. Yang, Z. W. Fu, *Electrochim. Commun.* **2012**, *16*, 22–25; c) N. Zhao, X. Guo, *J. Phys. Chem. C* **2015**, *119*, 25319–25326.
- [39] a) R. Pinedo, D. A. Weber, B. Bergner, D. Schröder, P. Adelhelm, J. Janek, *J. Phys. Chem. C* **2016**, *120*, 8472–8481; b) N. Zhao, C. Li, X. Guo, *Phys. Chem. Chem. Phys.* **2014**, *16*, 15646–15652.
- [40] L. Lutz, W. Yin, A. Grimaud, D. Alves Dalla Corte, M. Tang, L. Johnson, E. Azaceta, V. Sarou-Kanian, A. J. Naylor, S. Hamad, J. A. Anta, E. Salager, R. Tena-Zaera, P. G. Bruce, J. M. Tarascon, *J. Phys. Chem. C* **2016**, *120*, 20068–20076.
- [41] a) W. W. Yin, Z. Shadike, Y. Yang, F. Ding, L. Sang, H. Li, Z. W. Fu, *Chem. Commun.* **2015**, *51*, 2324–2327; b) W. Liu, Q. Sun, Y. Yang, J. Y. Xie, Z. W. Fu, *Chem. Commun.* **2013**, *49*, 1951–1953; c) W. Liu, W. Yin, F. Ding, L. Sang, Z. Fu, *Electrochim. Commun.* **2014**, *45*, 87–90; d) Q. Sun, H. Yadegari, M. N. Banis, J. Liu, B. Xiao, B. Wang, S. Lawes, X. Li, R. Li, X. Sun, *Nano Energy* **2015**, *12*, 698–708; e) F. Wu, Y. Xing, J. Lai, X. Zhang, Y. Ye, J. Qian, L. Li, R. Chen, *Adv. Funct. Mater.* **2017**, *27*, 1700632; f) J. L. Ma, N. Li, Q. Zhang, X. B. Zhang, J. Wang, K. Li, X. F. Hao, J. M. Yan, *Energy Environ. Sci.* **2018**, *11*, 2833–2838; g) N. Li, D. Xu, D. Bao, J. Ma, X. Zhang, *Chin. J. Catal.* **2016**, *37*, 1172–1179.
- [42] C. L. Bender, D. Schröder, R. Pinedo, P. Adelhelm, J. Janek, *Angew. Chem. Int. Ed.* **2016**, *55*, 4640–4649; *Angew. Chem.* **2016**, *128*, 4716–4726.
- [43] D. Schröder, C. L. Bender, R. Pinedo, W. Bartuli, M. G. Schwab, Ž. Tomović, J. Janek, *Energy Technol.* **2017**, *5*, 1242–1249.
- [44] a) L. Lutz, D. A. D. Corte, Y. Chen, D. Batuk, L. R. Johnson, A. Abakumov, L. Yate, E. Azaceta, P. G. Bruce, J.-M. Tarascon, A. Grimaud, *Adv. Energy Mater.* **2018**, *8*, 1701581; b) S. Ma, W. C. McKee, J. Wang, L. Guo, M. Jansen, Y. Xu, Z. Peng, *Phys. Chem. Chem. Phys.* **2017**, *19*, 12375–12383.
- [45] a) C. Sheng, F. Yu, Y. Wu, Z. Peng, Y. Chen, *Angew. Chem. Int. Ed.* **2018**, *57*, 9906–9910; *Angew. Chem.* **2018**, *130*, 10054–10058; b) I. M. Aldous, L. J. Hardwick, *Angew. Chem. Int. Ed.* **2016**, *55*, 8254–8257; *Angew. Chem.* **2016**, *128*, 8394–8397.
- [46] D. Schröder, C. L. Bender, R. Pinedo, W. Bartuli, M. G. Schwab, Ž. Tomović, J. Janek, *Energy Technol.* **2017**, *5*, 1242–1249.
- [47] P. Hartmann, M. Heinemann, C. L. Bender, K. Graf, R. P. Baumann, P. Adelhelm, C. Heiliger, J. Janek, *J. Phys. Chem. C* **2015**, *119*, 22778–22786.
- [48] a) H. Yadegari, C. J. Franko, M. N. Banis, Q. Sun, R. Li, G. R. Goward, X. Sun, *J. Phys. Chem. Lett.* **2017**, *8*, 4794–4800; b) J. Kim, H. Park, B. Lee, W. M. Seong, H. D. Lim, Y. Bae, H. Kim, W. K. Kim, K. H. Ryu, K. Kang, *Nanocomm.* **2016**, *7*, 10670; c) C. Xia, R. Fernandes, F. H. Cho, N. Sudhakar, B. Buonacorsi, S. Walker, M. Xu, J. Baugh, L. F. Nazar, *J. Am. Chem. Soc.* **2016**, *138*, 11219–11226; d) S. Y. Sayed, K. P. C. Yao, D. G. Kwabi, T. P. Batcho, C. V. Amanchukwu, S. Feng, C. V. Thompson, Y. Shao-Horn, *Chem. Commun.* **2016**, *52*, 9691–9694; e) C. Liu, M. Carboni, W. R. Brant, R. Pan, J. Hedman, J. Zhu, T. Gustafsson, R. Younesi, *ACS Appl. Mater. Interfaces* **2018**, *10*, 13534–13541.
- [49] N. Ortiz-Vitoriano, T. P. Batcho, D. G. Kwabi, B. Han, N. Pour, K. P. C. Yao, C. V. Thompson, Y. Shao-Horn, *J. Phys. Chem. Lett.* **2015**, *6*, 2636–2643.
- [50] W. J. Kwak, Z. Chen, C. S. Yoon, J. K. Lee, K. Amine, Y. K. Sun, *Nano Energy* **2015**, *12*, 123–130.
- [51] P. Adelhelm, P. Hartmann, C. L. Bender, M. Busche, C. Eufinger, J. Janek, *Beilstein J. Nanotechnol.* **2015**, *6*, 1016–1055.
- [52] C. L. Bender, P. Hartmann, M. Vračar, P. Adelhelm, J. Janek, *Adv. Energy Mater.* **2014**, *4*, 1301863.
- [53] S. Ma, W. C. McKee, J. Wang, L. Guo, M. Jansen, Y. Xu, Z. Peng, *Phys. Chem. Chem. Phys.* **2017**, *19*, 12375–12383.
- [54] a) Q. Sun, J. Liu, X. Li, B. Wang, H. Yadegari, A. Lushington, M. N. Banis, Y. Zhao, W. Xiao, N. Chen, J. Wang, T. K. Sham, X. Sun, *Adv. Funct. Mater.* **2017**, *27*, 1606662; b) X. Han, F. Cheng, C. Chen, F. Li, J. Chen, *Inorg. Chem. Front.* **2016**, *3*, 866–871.
- [55] M. Shang, Y. Liu, J. Xia, S. Zhang, J. Yang, *Ceram. Int.* **2017**, *43*, 3218–3223.
- [56] P. Hartmann, C. L. Bender, J. Sann, A. K. Dürr, M. Jansen, J. Janek, P. Adelhelm, *Phys. Chem. Chem. Phys.* **2013**, *15*, 11661–11672.
- [57] a) L. Lutz, W. Dachraoui, A. Demortière, L. R. Johnson, P. G. Bruce, A. Grimaud, J. M. Tarascon, *Nano Lett.* **2018**, *18*, 1280–1289; b) J. E. Nichols, B. D. McCloskey, *J. Phys. Chem. C* **2017**, *121*, 85–96.
- [58] C. Xia, R. Black, R. Fernandes, B. Adams, L. F. Nazar, *Nat. Chem.* **2015**, *7*, 496.
- [59] I. M. Aldous, L. J. Hardwick, *Chem. Commun.* **2018**, *54*, 3444–3447.
- [60] M. He, K. C. Lau, X. Ren, N. Xiao, W. D. McCulloch, L. A. Curtiss, Y. Wu, *Angew. Chem. Int. Ed.* **2016**, *55*, 15310–15314; *Angew. Chem.* **2016**, *128*, 15536–15540.
- [61] E. Azaceta, L. Lutz, A. Grimaud, J. M. Vicent-Luna, S. Hamad, L. Yate, G. Cabañero, H. J. Grande, J. A. Anta, J. M. Tarascon, R. Tena-Zaera, *ChemSusChem* **2017**, *10*, 1616–1623.
- [62] a) J. E. Nichols, K. B. Knudsen, B. D. McCloskey, *J. Phys. Chem. C* **2018**, *122*, 13462–13472; b) P. Hartmann, D. Grübl, H. Sommer, J. Janek, W. G. Bessler, P. Adelhelm, *J. Phys. Chem. C* **2014**, *118*, 1461–1471.
- [63] D. Schröder, C. L. Bender, M. Osenberg, A. Hilger, I. Manke, J. Janek, *Sci. Rep.* **2016**, *6*, 24288.
- [64] K. Li, S. R. Galle Kankanamge, T. K. Weldeghiorghis, R. Jorn, D. G. Kuroda, R. Kumar, *J. Phys. Chem. C* **2018**, *122*, 4747–4756.
- [65] R. Black, A. Shyamsunder, P. Adeli, D. Kundu, G. K. Murphy, L. F. Nazar, *ChemSusChem* **2016**, *9*, 1795–1803.
- [66] B. D. McCloskey, D. S. Bethune, R. M. Shelby, T. Mori, R. Scheffler, A. Speidel, M. Sherwood, A. C. Luntz, *J. Phys. Chem.* **2012**, *3*, 3043–3047.
- [67] H. Yadegari, M. Norouzi Banis, X. Lin, A. Koo, R. Li, X. Sun, *Chem. Mater.* **2018**, *30*, 5156–5160.
- [68] R. S. Assary, K. C. Lau, K. Amine, Y. K. Sun, L. A. Curtiss, *J. Phys. Chem. C* **2013**, *117*, 8041–8049.
- [69] E. Faktorovich-Simon, A. Natan, E. Peled, D. Golodnitsky, *J. Solid State Electrochem.* **2018**, *22*, 1015–1022.
- [70] V. Gutmann, E. Wychera, *Inorg. Nucl. Chem. Lett.* **1966**, *2*, 257–260.
- [71] Q. Shi, Y. Zhong, M. Wu, H. Wang, H. Wang, *Angew. Chem. Int. Ed.* **2018**, *57*, 9069–9072; *Angew. Chem.* **2018**, *130*, 9207–9210.
- [72] C. Liu, D. Rehnlund, W. R. Brant, J. Zhu, T. Gustafsson, R. Younesi, *ACS Energy Lett.* **2017**, *2*, 2440–2444.
- [73] N. B. Aetukuri, G. O. Jones, L. E. Thompson, C. Ozgit-Akgun, E. Akca, G. Demirci, H. C. Kim, D. S. Bethune, K. Virwani, G. M. Wallraff, *ACS Energy Lett.* **2018**, *3*, 2342–2348.
- [74] a) M. J. Lacey, J. T. Frith, J. R. Owen, *Electrochim. Commun.* **2013**, *26*, 74–76; b) L. Yang, J. T. Frith, N. Garcia-Araez, J. R. Owen, *Chem. Commun.* **2015**, *51*, 1705–1708.
- [75] W. W. Yin, J. L. Yue, M. H. Cao, W. Liu, J. J. Ding, F. Ding, L. Sang, Z. W. Fu, *J. Mater. Chem. A* **2015**, *3*, 19027–19032.
- [76] J. T. Frith, I. Landa-Medrano, I. Ruiz De Laramendi, T. Rojo, J. R. Owen, N. Garcia-Araez, *Chem. Commun.* **2017**, *53*, 12008–12011.
- [77] a) D. R. MacFarlane, N. Tachikawa, M. Forsyth, J. M. Pringle, P. C. Howlett, G. D. Elliott, J. H. Davis, M. Watanabe, P. Simon, C. A. Angell, *Energy Environ. Sci.* **2014**, *7*, 232–250; b) Y. Zhang, C. Pozo-Gonzalo, *Chem. Commun.* **2018**, *54*, 3800–3810.
- [78] Y. Yan, D. Gunzelmann, C. Pozo-Gonzalo, A. F. Hollenkamp, P. C. Howlett, D. R. MacFarlane, M. Forsyth, *Electrochim. Acta* **2017**, *235*, 270–279.

- [79] a) C. Pozo-Gonzalo, L. R. Johnson, E. Jónsson, C. Holc, R. Kerr, D. R. MacFarlane, P. G. Bruce, P. C. Howlett, M. Forsyth, *J. Phys. Chem. C* **2017**, *121*, 23307–23316; b) C. Pozo-Gonzalo, P. C. Howlett, D. R. MacFarlane, M. Forsyth, *Electrochem. Commun.* **2017**, *74*, 14–18.
- [80] Y. Katayama, H. Onodera, M. Yamagata, T. Miura, *J. Electrochem. Soc.* **2004**, *151*, A59–A63.
- [81] Y. Zhang, N. Ortiz-Vitoriano, B. Acebedo, L. O'Dell, D. R. MacFarlane, T. Rojo, M. Forsyth, P. C. Howlett, C. Pozo-Gonzalo, *J. Phys. Chem. C* **2018**, *122*, 15276–15286.
- [82] a) L. Suo, Y. S. Hu, H. Li, M. Armand, L. Chen, *Nat. Commun.* **2013**, *4*, 1481; b) W. Walker, V. Giordani, J. Uddin, V. S. Bryantsev, G. V. Chase, D. Addison, *J. Am. Chem. Soc.* **2013**, *135*, 2076–2079.
- [83] R. Tatara, G. M. Leverick, S. Feng, S. Wan, S. Terada, K. Dokko, M. Watanabe, Y. Shao-Horn, *J. Phys. Chem. C* **2018**, *122*, 18316–18328.
- [84] "Battery Energy Storage System Market by Element (Battery, Hardware), Battery Type (Lithium-Ion, Advanced Lead Acid, Flow Batteries, Sodium Sulfur), Connection Type (On-Grid and Off-Grid), Ownership, Application, and Geography - Global Forecast to 2023" can be found under <https://www.marketsandmarkets.com/Market-Reports/battery-energy-storage-system-market-112809494.html>

Manuscript received: January 13, 2019

Revised manuscript received: April 8, 2019

Accepted manuscript online: April 23, 2019

Version of record online: June 28, 2019
